



Electron scattering by whistler-mode ELF hiss in plasmaspheric plumes

Danny Summers,¹ Binbin Ni,¹ Nigel P. Meredith,² Richard B. Horne,² Richard M. Thorne,³ Mark B. Moldwin,⁴ and Roger R. Anderson⁵

Received 23 July 2007; revised 27 October 2007; accepted 14 January 2008; published 23 April 2008.

[1] Nonadiabatic loss processes of radiation belt energetic electrons include precipitation loss to the atmosphere due to pitch-angle scattering by various magnetospheric plasma wave modes. Here we consider electron precipitation loss due to pitch-angle scattering by whistler-mode ELF hiss in plasmaspheric plumes. Using wave observations and inferred plasma densities from the Plasma Wave Experiment on the Combined Release and Radiation Effects Satellite (CRRES), we analyze plume intervals for which well-determined hiss spectral intensities are available. We then select 14 representative plumes for detailed study, comprising 10 duskside plumes and 4 nonduskside plumes, with local hiss amplitudes ranging from maximum values of above 300 pT to minimum values of less than 1 pT. We estimate the electron loss timescale τ_{loss} due to pitch-angle scattering by hiss in each chosen plume as a function of L -shell and electron energy; τ_{loss} is calculated from quasi-linear theory as the inverse of the bounce-averaged diffusion rate evaluated at the equatorial loss cone angle. We find that pitch-angle scattering by hiss in plumes can be efficient for inducing precipitation loss of outer-zone electrons with energies throughout the range 100 keV to 1 MeV, though the magnitude of τ_{loss} can be highly dependent on wave power, L -shell, and electron energy. For 100- to 200-keV electrons, typically $\tau_{loss} \sim 1$ day while the minimum loss timescale $(\tau_{loss})_{min} \sim$ hours. For 500-keV to 1-MeV electrons, typically $(\tau_{loss})_{min} \sim$ days, while $(\tau_{loss})_{min} < 1$ day in the case of large wave amplitude (~ 100 's pT). Apart from inducing direct precipitation loss of MeV electrons, scattering by hiss in plumes may reduce the generation of MeV electrons by depleting the lower energy electron seed population. Models of the dynamical variation of the outer-zone electron flux should incorporate electron precipitation loss induced by ELF hiss scattering in plasmaspheric plumes.

Citation: Summers, D., B. Ni, N. P. Meredith, R. B. Horne, R. M. Thorne, M. B. Moldwin, and R. R. Anderson (2008), Electron scattering by whistler-mode ELF hiss in plasmaspheric plumes, *J. Geophys. Res.*, 113, A04219, doi:10.1029/2007JA012678.

1. Introduction

[2] In order to understand and quantify energetic electron flux variations in the inner magnetosphere, it is necessary to assess both the electron energization and loss processes. Loss mechanisms may be adiabatic, which are temporary, or nonadiabatic which result in net particle loss. Nonadiabatic loss processes include precipitation loss to the atmosphere due to pitch-angle scattering by plasma waves, and loss due

to particle drift across the magnetospheric boundary. Radiation belt electrons can undergo gyroresonant pitch-angle scattering by various wave modes, including whistler-mode VLF chorus, plasmaspheric ELF hiss, and electromagnetic ion cyclotron (EMIC) waves [e.g., see *Summers et al.*, 2007a, 2007b, and references therein]. In the present paper we analyze a particular form of electron precipitation loss, namely that due to pitch-angle scattering by ELF hiss in plasmaspheric plumes.

[3] The plasmasphere is a cold (a few eV), dense ($10\text{--}10^4\text{ cm}^{-3}$) plasma torus surrounding the Earth in the innermost magnetosphere [e.g., *Carpenter*, 1963; *Chappell et al.*, 1970; *Carpenter and Park*, 1973; *Horwitz et al.*, 1990; *Carpenter and Lemaire*, 1997; *Lemaire and Gringauz*, 1998; *Ganguli et al.*, 2000; *Goldstein*, 2006; *Dent et al.*, 2006]. The multi-ion (H^+ , He^+ , O^+) plasma comprising the plasmasphere derives from the ionosphere and corotates with the Earth. The region of cold plasma rotation and the overall shape of the plasmasphere are controlled by the interaction of the corotational electric field and the solar wind influenced dawn-to-dusk cross-tail

¹Department of Mathematics and Statistics, Memorial University of Newfoundland, St. John's, Newfoundland, Canada.

²British Antarctic Survey, Natural Environment Research Council, Cambridge, UK.

³Department of Atmospheric and Oceanic Sciences, University of California, Los Angeles, California, USA.

⁴Institute of Geophysics and Planetary Physics and Department of Earth and Space Sciences, University of California, Los Angeles, California, USA.

⁵Department of Physics and Astronomy, University of Iowa, Iowa City, Iowa, USA.

electric field. During intense geomagnetic storms the plasmaspheric boundary layer, or plasmopause, can lie inside $L = 2$ for several days [Baker et al., 2004], while during prolonged periods of quiet geomagnetic conditions the plasmasphere can extend to beyond geosynchronous orbit ($L \sim 6.6$) and possess no distinct outer boundary [Goldstein et al., 2003]. Following geomagnetically disturbed periods, and as a result of interplay between forces driving the plasma sunward and corotational forces, plasma typically drains from the body of the plasmasphere in the afternoon local time sector. The resulting large-scale plasma structures which stretch toward the outer magnetosphere are usually attached to the plasmasphere and are called plasmaspheric plumes or plasmaspheric drainage plumes. Historically, they have been called tails [Taylor et al., 1971] or detached plasma elements (or blobs) [Chappell, 1974]. Using plasma density data inferred from the Plasma Wave Experiment on the Combined Release and Radiation Effects Satellite (CRRES), Moldwin et al. [2004] found that plumes can exist at all local times under all levels of geomagnetic activity, but that most were observed in the noon-to-dusk sector following enhanced geomagnetic activity. In many of the methods hitherto used it should be noted that whether or not the observed plasma structures were attached to the plasmasphere could not easily be determined. Excellent global images of evolving plasmaspheric plumes have been provided by the extreme ultraviolet (EUV) imager of the Imager for Magnetopause-to-Aurora Global Exploration (IMAGE) satellite [e.g., Sandel et al., 2003; Goldstein et al., 2003, 2004, 2005; Spasojević et al., 2003, 2004; Burch, 2006; Goldstein, 2006]. In situ measurements from the four CLUSTER satellites confirm that plumes rotate around the Earth, with their feet attached to the main plasmasphere fully corotating, but with their tips often rotating more slowly and moving outward away from the Earth [Darrouzet et al., 2006].

[4] Plasmaspheric hiss is a broadband ELF electromagnetic whistler-mode emission which occurs in the frequency range from ~ 100 Hz to several kHz. Hiss is present over a broad region of the plasmasphere even during geomagnetically quiet periods and intensifies during storms or substorms [Smith et al., 1974; Thorne et al., 1974; Meredith et al., 2004]. Broadband amplitudes of hiss range from 10 pT or below during quiet periods to ~ 100 's pT during disturbed times [Smith et al., 1974; Tsurutani et al., 1975; Meredith et al., 2004]. Hiss is generally field-aligned near the magnetic equator and tends to propagate more obliquely at higher latitudes [Parrot and Lefeuvre, 1986; Santolik et al., 2001]. There are extensive observations of plasmaspheric hiss [e.g., see Hayakawa and Sazhin, 1992; Meredith et al., 2004; Masson et al., 2004, and references therein]. Whistler-mode hiss has also been observed in plasmaspheric plumes [Chan and Holzer, 1976; Cornilleau-Wehrin et al., 1978; Hayakawa et al., 1986; Parrot and Lefeuvre, 1986]. Analyzing CRRES wave and particle data, Meredith et al. [2004] found that plasmaspheric hiss peaks in particular equatorial ($|\text{MLAT}| < 15^\circ$) and midlatitude ($15^\circ < |\text{MLAT}| < 30^\circ$) regions, mainly on the dayside, and that generally hiss amplitudes depend on L -shell, MLT and magnetic latitude, as well as substorm activity. Plasmaspheric hiss, together with other whistler-mode emissions [Abel and Thorne, 1998], plays an impor-

tant role in controlling the structure of the Earth's radiation belts. Lyons and Thorne [1973] showed that the formation of the quiet-time slot region between the inner ($1.3 < L < 2.5$) and outer ($3 < L < 7$) radiation belts can be explained as an equilibrium balance between inward radial diffusion and pitch-angle scattering loss of energetic electrons to the atmosphere induced by plasmaspheric hiss [Lyons et al., 1972]. Plasmaspheric hiss can also cause scattering loss of MeV electrons from the outer radiation belt over a timescale of days, or less, under appropriate conditions [Tsurutani et al., 1975; Albert, 1994, 2003; Summers et al., 2007b]. Meredith et al. [2006a] used CRRES data to measure the gradual decay of energetic (214 keV to 1.09 MeV) electron fluxes in the outer zone following enhanced geomagnetic activity. Meredith et al. [2006a] and Summers et al. [2007b] found that scattering by plasmaspheric hiss propagating at zero or small wave normal angles could account for the measured electron decay rates over a wide range of energies and L -shells.

[5] The generation mechanism of plasmaspheric hiss has not been fully resolved and remains controversial. There are two leading theories for the source of plasmaspheric hiss, namely, in situ natural instability in the magnetosphere [e.g., Etcheto et al., 1973; Thorne et al., 1979; Huang et al., 1983], and lightning-generated whistlers [e.g., Sonwalkar and Inan, 1989; Draganov et al., 1992; Green et al., 2005]. The analysis by Green et al. [2005] supporting lightning as the dominant source for plasmaspheric hiss was disputed by Thorne et al. [2006]; see also the reply by Green et al. [2006]. Meredith et al. [2006b] subsequently analyzed the entire CRRES database of plasmaspheric hiss together with the global distribution of lightning and concluded that while higher-frequency hiss (2–5 kHz) is generated by lightning, lower frequency hiss (100 Hz to 2 kHz) is generated by natural instability in space. Evidence that lower frequency hiss intensifies during enhanced geomagnetic activity [e.g., Meredith et al., 2004] points to natural instability as the origin of lower frequency hiss.

[6] There is increasing interest in wave-particle interactions occurring in plasmaspheric plumes with respect to their role in influencing particle dynamics in the inner magnetosphere. Pitch-angle scattering by EMIC waves in plumes can cause significant precipitation loss of energetic protons [Burch et al., 2002; Spasojević et al., 2004; Burch, 2006]. Summers et al. [2007b] and Summers and Ni [2008] found that an assumed realistic spatial distribution of EMIC waves and hiss in an empirically measured plume could induce rapid scattering loss of outer zone electrons. The relative contributions to electron scattering by hiss and EMIC waves in plumes depend on the electron energy and L -shell, as well as the wave properties [see Summers et al., 2007b, Figures 21 and 22], and Summers and Ni [2008, Figures 9 and 10]. In the present paper we analyze hiss-electron interaction in plasmaspheric plumes selected from the CRRES mission. Specifically, we determine intervals during which CRRES crossed a plume and select a subset of plume intervals for which well-observed hiss data are available. We then use quasi-linear theory to determine hiss-induced pitch-angle scattering rates at the loss cone for electrons of specified energy at given L -values. We can thereby estimate timescales for precipitation loss of energetic electrons in the inner magnetosphere due to scattering

by hiss in plumes. The present study is the first to determine electron precipitation loss timescales due to scattering by measured hiss in observed plumes. We present our selection of plume intervals and associated hiss data in section 2. In section 3 we summarize the necessary quasi-linear theory required for our calculations. In section 4 we present our estimates for electron loss timescales due to scattering by hiss in the chosen plumes. Finally, in section 5 we discuss the significance of our results.

2. CRRES Plume and Wave Observations

[7] CRRES was launched on 25 July 1990 and functioned until 12 October 1991. The spacecraft had a geosynchronous transfer orbit, namely an elliptical orbit with a perigee of $1.05 R_E$ and an apogee of $6.26 R_E$ with respect to the Earth's center, with an inclination of 18.15° . The outermost L -shell reached by CRRES was $L \sim 8$. The orbital period was approximately 9 hours 55 minutes, and the apogee of CRRES precessed from 10.00 MLT to 14.00 MLT through midnight before the mission terminated. The satellite was able to provide excellent coverage of the radiation belts for nearly 15 months since it traversed the inner magnetosphere on average about 5 times per day. The wave data and plasma densities used in this study were obtained from the Plasma Wave Experiment (PWE) on board CRRES. This experiment measured electric fields from 5.6 Hz to 400 kHz, using a 100 m tip-to-tip long wire antenna, with a dynamic range covering a factor of at least 10^5 in amplitude [Anderson *et al.*, 1992]. The electric field detector was thus able to detect waves from below the lower hybrid resonance frequency (f_{LHR}) to well above the upper hybrid resonance frequency (f_{UHR}) for a large fraction of each orbit. The maximum plasma density that could be measured was $\sim 2000 \text{ cm}^{-3}$ because of the upper frequency limit of the instrument. The CRRES PWE also included a boom-mounted search coil magnetometer that covered the frequency range from 5.6 Hz to 10 kHz and operated until the March 1991 storm. While the electric field data were sampled with high-frequency resolution by the PWE sweep frequency receiver at eight seconds per spectra above 6.4 kHz, the search coil data were sampled by a 14-channel analyzer that sampled the magnetic field eight times per second every other 32 seconds.

[8] We determine the presence of a plume by monitoring the behavior of the plasma density as inferred from observations of the upper hybrid resonance frequency. If, while CRRES is clearly outside the plasmasphere, the density suddenly increases, remains high for some time, and then suddenly decreases, we identify the region as a potential plume. We refer to such a region as a plume for simplicity, even though CRRES observations cannot determine if the identified high-density region is attached to the plasmasphere. We also use the absence of electrostatic electron cyclotron harmonic (ECH) waves as a criterion for identifying high-density plasma regions, as described by Meredith *et al.* [2004]. Identification of a plume and its boundary can be problematic observationally, and is, to a degree, subjective. Determination of a boundary of a plume is straightforward if it is sharp, and difficult if it is gradual. This situation likewise applies to the determination of the boundary of the plumpause itself. To complement the techniques

applied for identifying plumes in our study, we also make use of the rigorous plume selection criteria of Moldwin *et al.* [2004]. The comprehensive study of plumes during the CRRES mission by Moldwin *et al.* [2004] employed the database of plumpause locations identified by Moldwin *et al.* [2002] and the empirical plasmaspheric and trough density models developed by Sheeley *et al.* [2001]. These three studies used a common database of plasma density derived from the CRRES Plasma Wave Experiment. Moldwin *et al.* [2002] identified the innermost steep density gradient in the density profile as the plumpause, a factor of 5 drop within half an L -shell being required. In order to select intervals of enhanced density located outside the plumpause, Moldwin *et al.* [2004] used $L = 3$ as a dividing line for whether to use the plasmaspheric or trough density model. If the plumpause is located earthward of $L = 3$, plasmaspheric plume intervals are defined as those whose density exceeds the trough plus one standard deviation density of the Sheeley *et al.* [2001] model. If the plumpause is located outside of $L = 3$, plasmaspheric plume intervals are defined as those whose density exceeds the Sheeley *et al.* [2001] plasmaspheric model. These models are scaled to each orbit to account for the wide variability in the plasmaspheric density from day to day. The criterion used by Moldwin *et al.* [2004] to select a plume is that the density throughout the requisite interval must exceed the model value of the plasmaspheric density (or trough plus one standard deviation) over a minimum of 8 consecutive observations (a duration of ~ 1 min).

[9] In our study we choose 14 plume intervals which we specify in Table 1, according to orbit number, by giving the start and end values of universal time (UT), magnetic local time (MLT), L -shell, and magnetic latitude (MLAT). We have chosen 10 plumes with a duskside MLT location, namely crossed by outbound CRRES orbits 605, 672, 673, 674, 810, 869, 871, 939, 941, and 977. The remaining 4 plumes, crossed by outbound orbits 302 and 446, and inbound orbits 297 and 446, are nonduskside. The 14 chosen plume crossings are illustrated in Figure 1 in which we also show the approximate trajectory for CRRES orbit 446. Our chosen plumes were likewise identified as plumes by Moldwin *et al.* [2004], with the exception of the 3 plumes associated with orbits 297 and 446. These latter plumes were not selected in the Moldwin *et al.* [2004] study because the density did not satisfy their conservative plasmaspheric density criteria. We nevertheless regard these features as representative nonduskside plumes because of their distinctly elevated densities compared to the surrounding trough.

[10] In some of the selected plumes common to the present study and that of Moldwin *et al.* [2004], the specified start and end of the plume interval, as for instance given by L -shell, differ slightly because of the differing plume boundary criteria used in the two studies. This issue does not lead to serious difficulties in our investigation since we base the conclusions of our analysis on electron loss timescales that are calculated well inside each plume. Thus, possibly spurious edge effects are readily eliminated.

[11] We show measured CRRES electron density profiles corresponding to the outbound (blue) and inbound (red) portions of orbits 446, 869, 939, and 977 in Figures 2a, 2b, 2c, and 2d, respectively. For comparison purposes, in each plot we also show upper and lower black curves represent-

Table 1. Specification of the 14 CRRES Plume Crossings Chosen in This Study^a

ORBIT	UT (start)	UT (end)	MLT (start)	MLT (end)	L (start)	L (end)	MLAT (start)	MLAT (end)
297 (<i>In</i>)	01:58	04:02	03:55	05:44	6.43	4.18	12.8	7.1
302 (<i>Out</i>)	22:01	23:35	23:17	01:28	3.26	5.86	15.4	16.3
446 (<i>Out</i>)	00:31	01:15	21:22	22:18	4.41	5.63	26.7	23.7
446 (<i>In</i>)	05:22	07:16	01:06	02:47	6.72	4.76	13.8	6.75
605 (<i>Out</i>)	05:03	06:43	19:14	20:45	4.15	6.05	4.9	-2.6
672 (<i>Out</i>)	15:33	15:48	18:14	18:33	4.45	4.85	-8.5	-9.9
673 (<i>Out</i>)	00:53	01:26	17:35	18:25	3.55	4.45	6.7	3.3
674 (<i>Out</i>)	11:08	11:48	18:09	18:55	4.45	5.55	-15.4	-18.5
810 (<i>Out</i>)	17:30	19:23	15:54	17:43	4.15	6.25	-6.0	-9.0
869 (<i>Out</i>)	00:54	02:46	16:07	17:14	5.65	6.85	-13.9	-14.5
871 (<i>Out</i>)	20:33	22:44	15:05	16:54	4.25	6.35	-7.1	-7.4
939 (<i>Out</i>)	01:12	02:16	13:49	14:48	4.95	6.15	-20.2	-18.8
941 (<i>Out</i>)	21:31	22:26	13:25	14:30	4.05	5.25	-11.8	-10.3
977 (<i>Out</i>)	09:30	11:00	13:06	14:16	5.85	6.65	-21.8	-17.7

^aThe magnetic latitude (MLAT) is given in degrees; UT is universal time and MLT is magnetic local time.

ing respectively the saturated plasmasphere density and trough density given by the *Carpenter and Anderson* [1992] model. The plume intervals for orbits 446, 869, 939, and 977 as specified by L -shell range in Table 1 can be observed to match the corresponding intervals of elevated density in Figures 2a–2d.

[12] In Figure 3 the measured wave electric field spectral intensities (in $V^2 m^{-2} Hz^{-1}$) are plotted as a function of UT for the complete CRRES orbits 446 and 869. Similar wave plots are given for orbits 939 and 977 in Figure 4. The

magnetic local time, magnetic latitude, and L -shell are given at hourly intervals. The solid white line shows the value of the electron gyrofrequency f_{ce} , determined from the measured ambient magnetic field, and the dashed white lines below f_{ce} represent $0.5f_{ce}$, $0.1f_{ce}$, and the lower hybrid resonance frequency, f_{LHR} . The dotted white lines above f_{ce} correspond to the first four harmonics of f_{ce} . The solid red line denotes the upper hybrid resonance frequency $f_{UHR} = (f_{pe}^2 + f_{ce}^2)^{1/2}$ (where f_{pe} is the electron plasma frequency) calculated from the lower frequency cut-off of the electro-

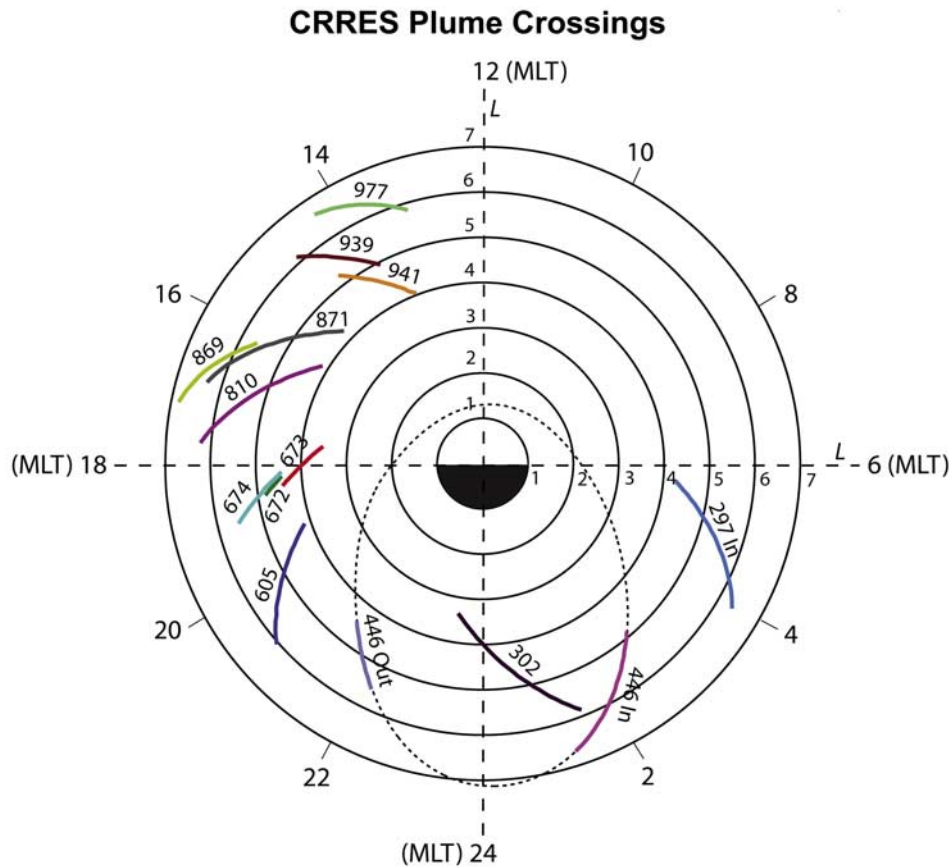


Figure 1. Diagram showing the 14 CRRES plume crossings identified by orbit number, chosen in this study. All the chosen plumes correspond to outbound portions of the specified orbits, except for the indicated 297 (*In*) and 446 (*In*) inbound crossings. Also shown is an approximate trajectory for CRRES orbit 446.

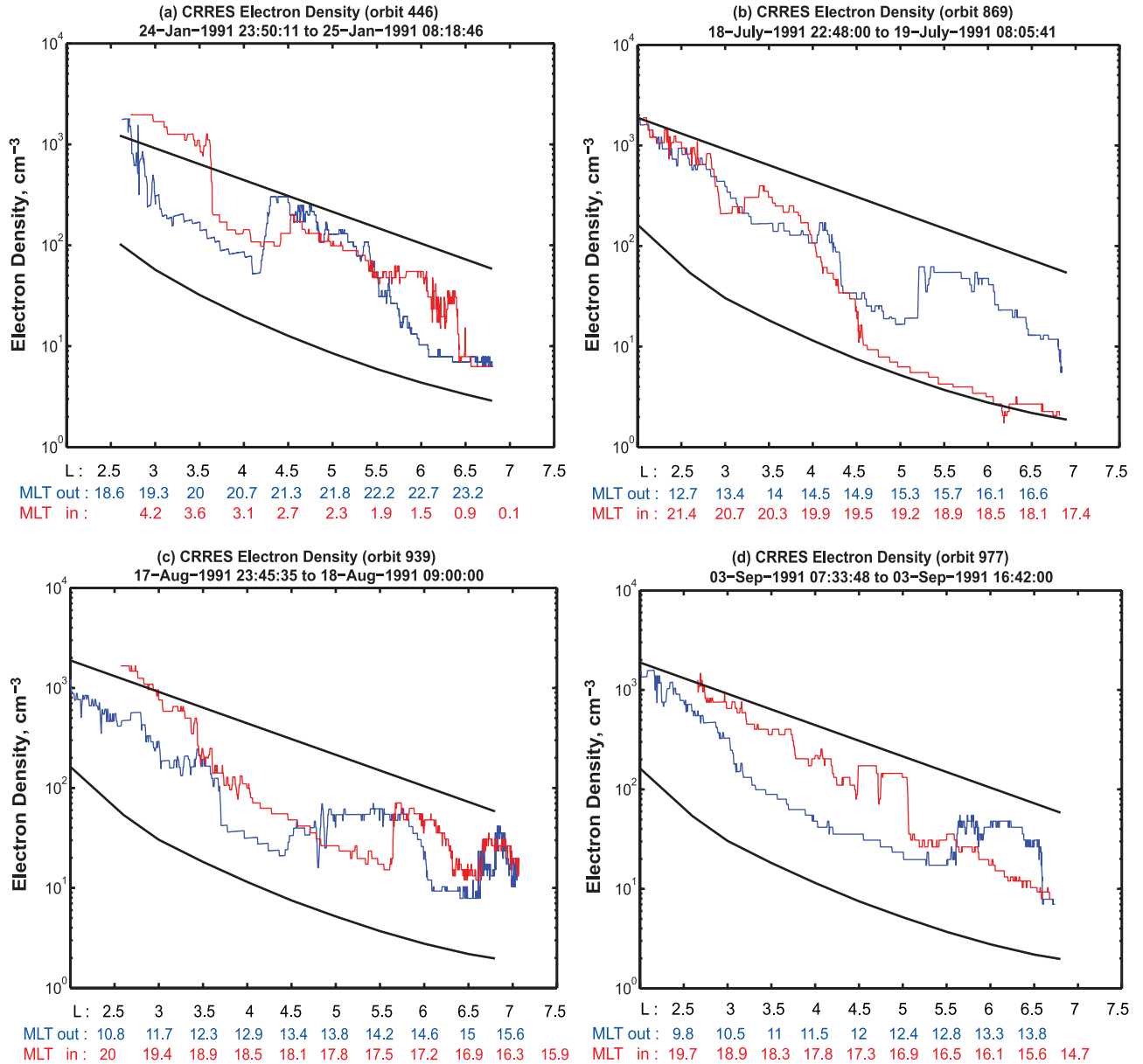


Figure 2. Measured CRRES electron density profiles for orbits 446, 869, 939, and 977. Chosen plume intervals during these orbits are specified in Table 1. The upper and lower black curves in each plot are model profiles of the saturated plasmasphere density and trough density from *Carpenter and Anderson [1992]*.

magnetic continuum, and the red dashed line represents f_{UHR} calculated from wave emissions at f_{UHR} inside the plasmopause. The chosen plumes in the orbits 446 and 869 are indicated in Figure 3, together with their associated hiss emissions. Likewise, the chosen plumes in orbits 939 and 977 and their hiss emissions are indicated in Figure 4. Profiles of the AE index are provided at one-minute time resolution. The empirical position of the plasmopause as defined by *Carpenter and Anderson [1992]* is also marked.

[13] We base the calculations in our study on hiss in the frequency range $104 < f < 1040$ Hz. The general criterion used in this paper to identify hiss in plumes is that used by *Meredith et al. [2004]* to identify plasmaspheric hiss, namely, ECH wave amplitudes for frequencies in the range

$f_{ce} < f < 2f_{ce}$ must be less than 0.0005 mV m^{-1} in order for wave emissions below f_{ce} in the frequency band $104 < f < 1040$ Hz to be identified as hiss. Whistler-mode chorus has a frequency range $0.3 < f < 30$ kHz in the region $3 < L < 7$. Consequently, chorus can lie in our chosen hiss frequency band at higher L -shells. However, whistler-mode chorus is usually observed outside the plasmasphere and high-density regions so can be excluded from consideration in our chosen plumes. At lower L -shells, magnetosonic waves can also fall into our chosen hiss frequency band. These waves, which are closely confined to the equatorial region, are enhanced during active conditions below the lower hybrid resonance frequency f_{LHR} , represented by the lowest dashed line in the spectrograms in Figures 3 and 4. We find

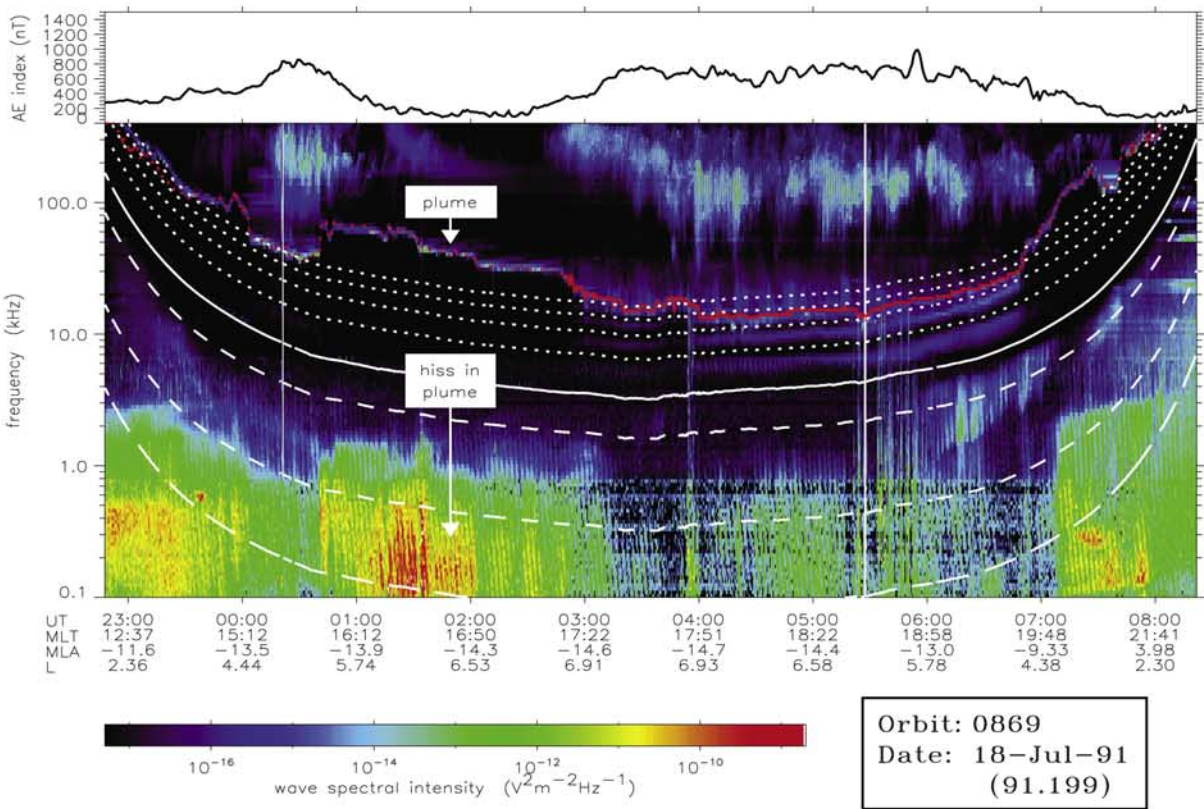
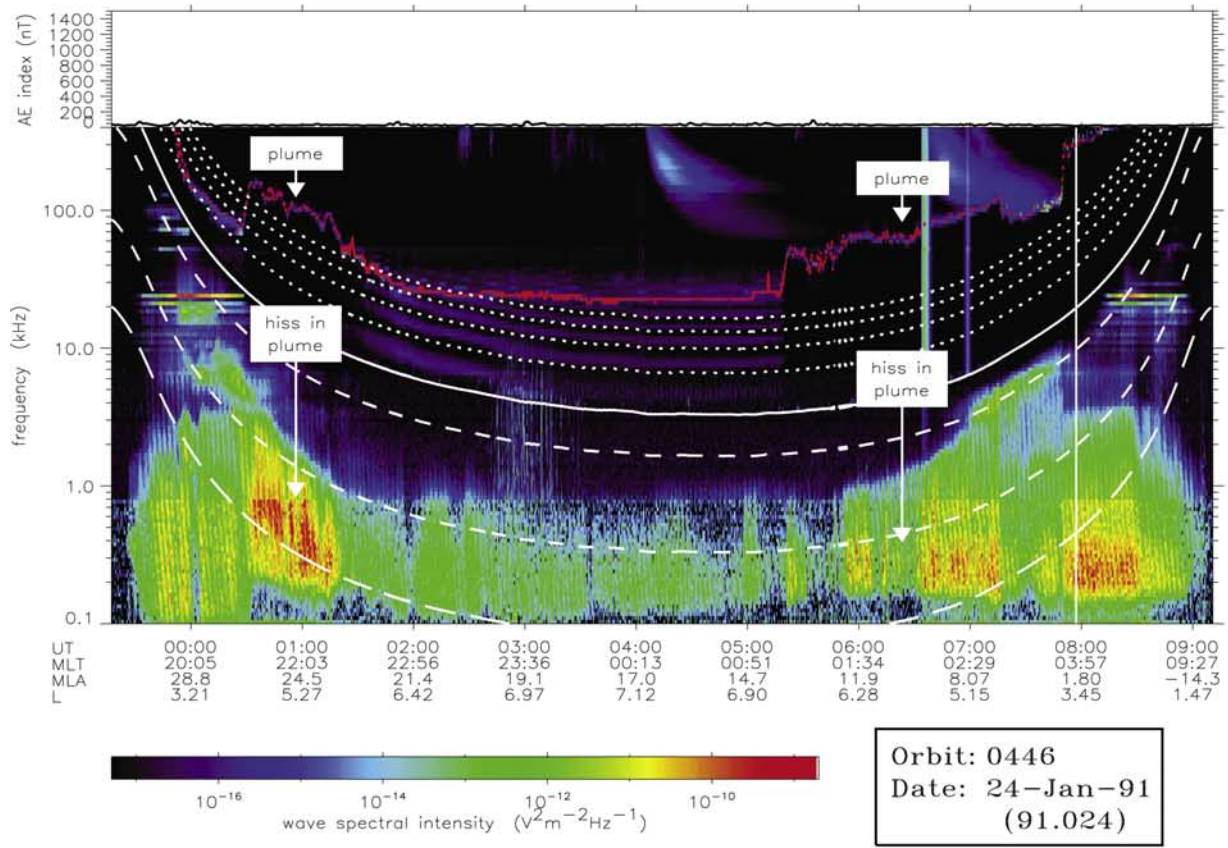


Figure 3. Survey plot of the wave spectral intensities observed on CRRES for orbits (top) 446 and (bottom) 869.

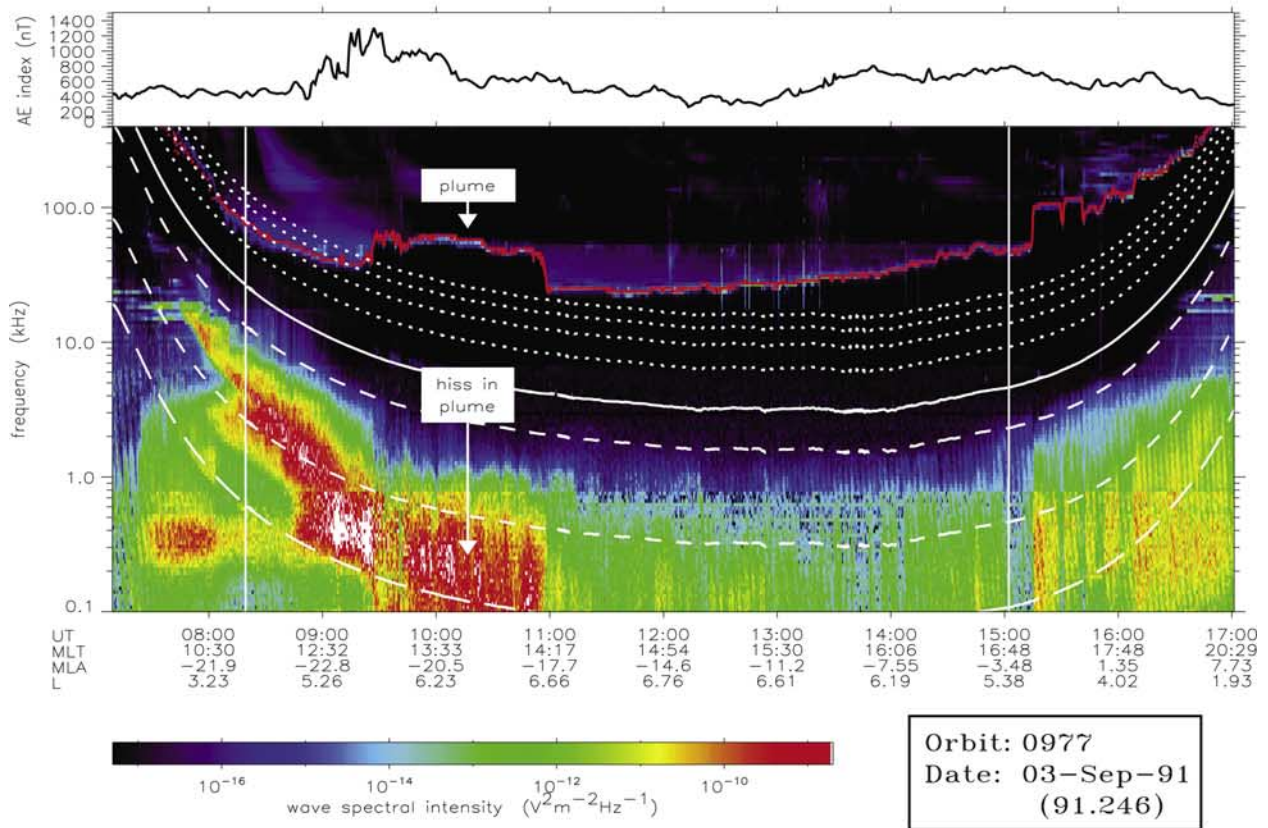
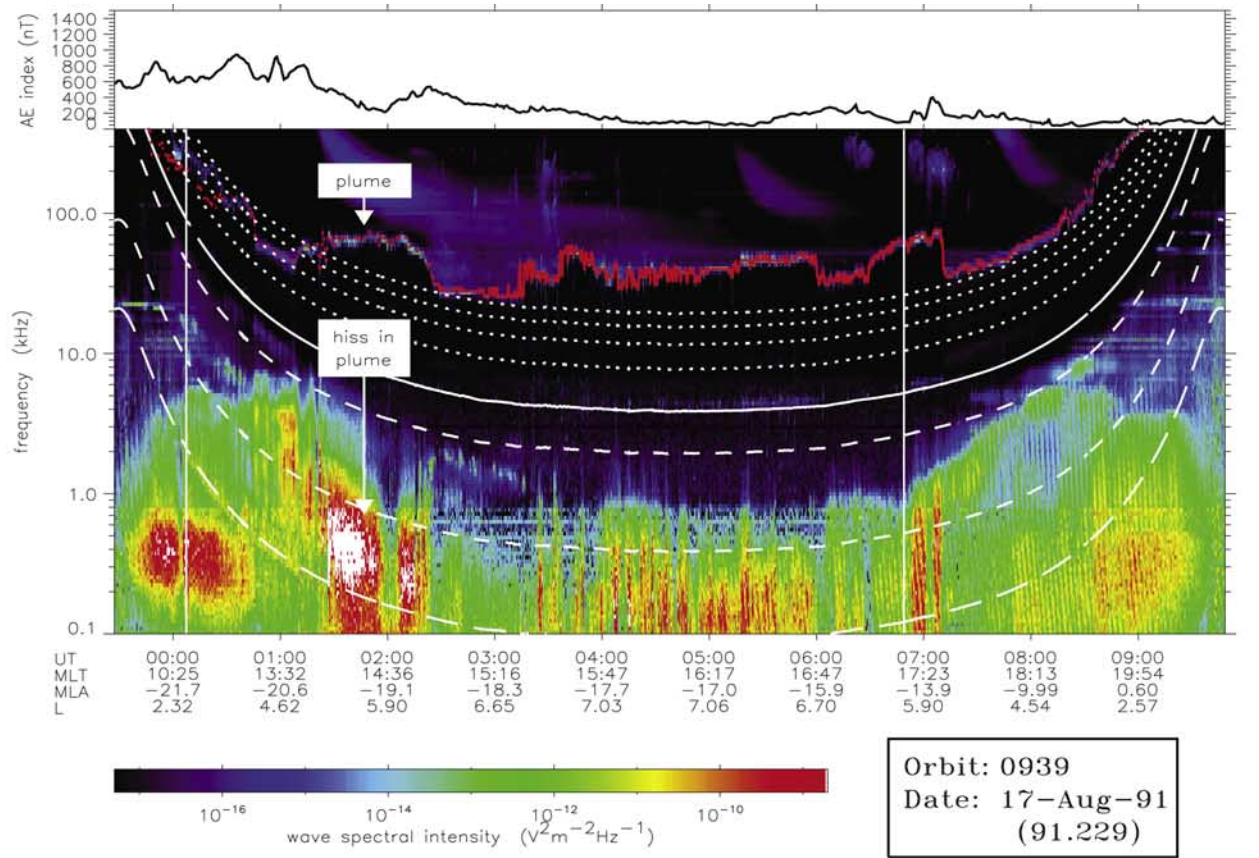


Figure 4. Survey plot of the wave spectral intensities observed on CRRES for orbits (top) 939 and (bottom) 977.

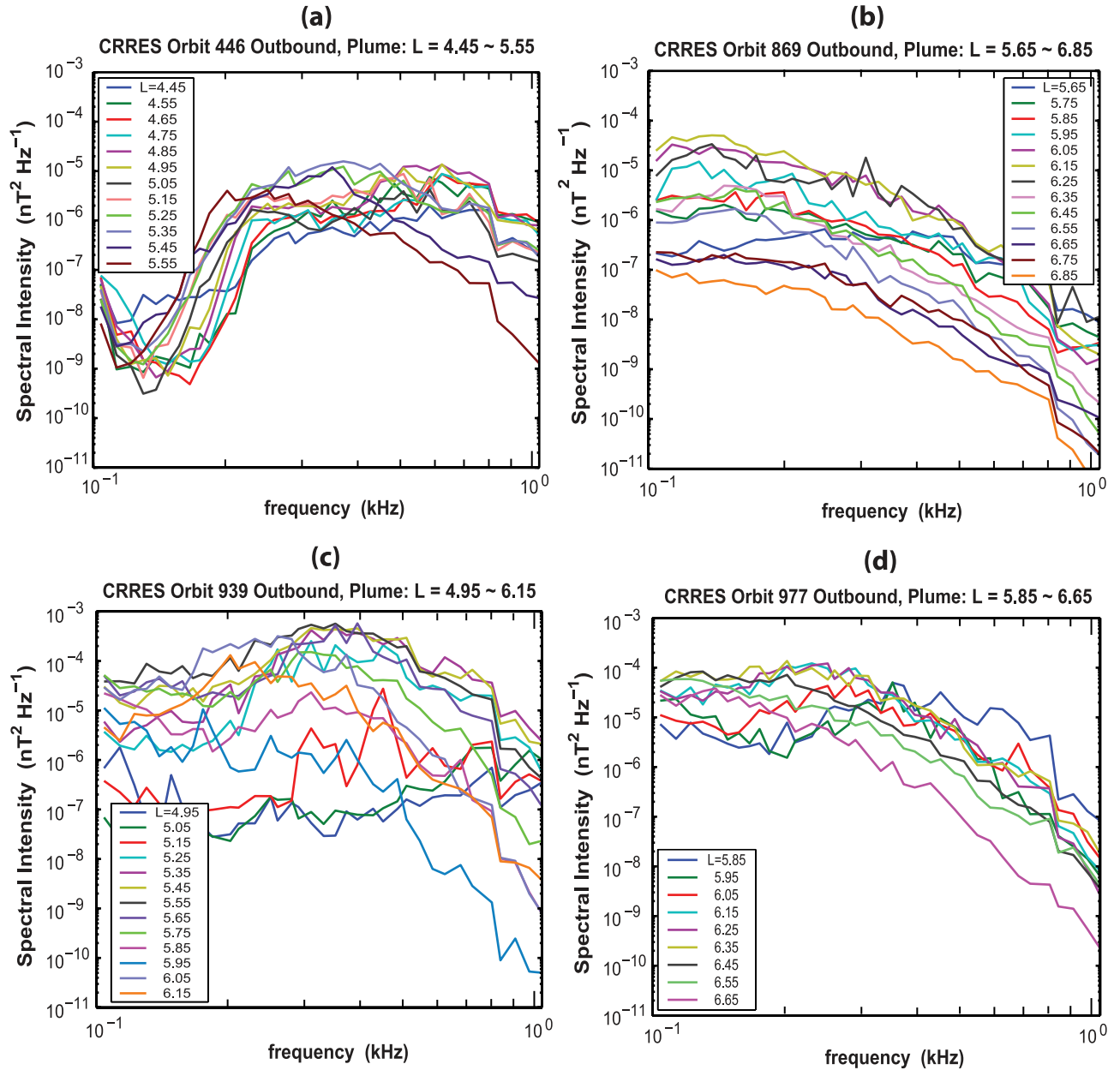


Figure 5. Measured hiss spectral intensities at the indicated L -values during the chosen plume crossings from CRRES orbits (a) 446 (Out), (b) 869, (c) 939, and (d) 977.

no evidence of enhanced magnetosonic waves within our chosen plumes, except possibly during orbit 871. For the chosen plume in this orbit, hiss intensities may be slightly overestimated in the region $4.25 < L < 5.25$ as a result of contamination by magnetosonic waves.

[14] In order to convert observed hiss electric field spectral intensities to magnetic field intensities, we use a cold-plasma dispersion relation for parallel-propagating whistler-mode waves (equation (4) of section 3, with $\varepsilon = 0$), Maxwell's induction equation, and expression (1) given by Meredith *et al.* [2004]. Magnetic field wave intensities over the frequency range $104 < f < 1040$ Hz are then defined as an integral of the averaged wave spectral intensity ($\text{nT}^2 \text{Hz}^{-1}$). The corresponding wave amplitudes are obtained by taking the square root of the wave intensities,

as detailed in section 3. Conversion from electric to magnetic fields is relatively insensitive to wave normal angle for wave normal angles less than 50° , if $f < 0.5f_{ce}$ [Meredith *et al.*, 2004]. We discuss our assumption of parallel wave propagation further below.

[15] We present hiss spectral intensities in $\text{nT}^2 \text{Hz}^{-1}$ within four chosen plumes during orbits 446, 869, 939, and 977, in Figures 5a, 5b, 5c, and 5d, respectively. In each plot the spectral intensity is shown at a range of specified L -shells within the plume. In Figure 6 we show the measured values of the local hiss amplitudes at the given L -shells within each of our 14 chosen plume intervals. Local wave amplitudes range from maximum values that exceed 300 pT, for the plumes in orbits 810 and 939, to minimum values of less than 1 pT, in orbits 297, 446(In), and 810.

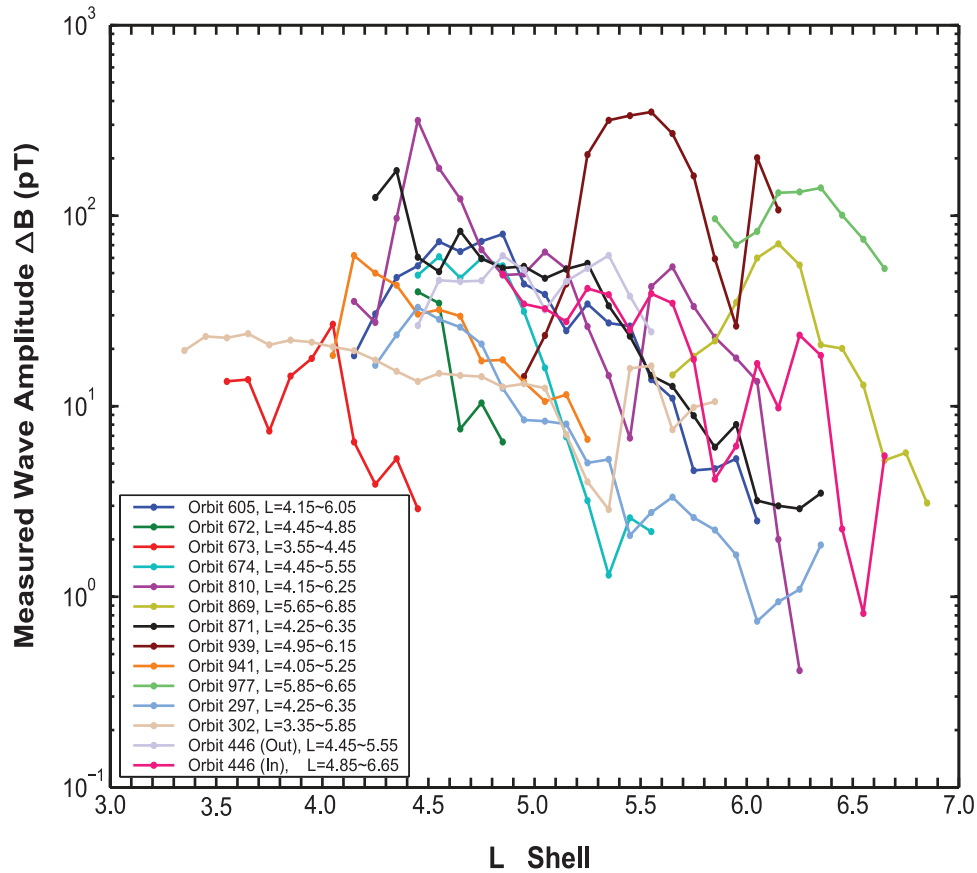


Figure 6. Local hiss amplitude in the frequency range 104–1040 Hz measured by CRRES along each chosen plume crossing.

This probably represents the widest range of hiss amplitudes to be expected in plasmaspheric plumes. Further, since we have mainly chosen more commonly occurring duskside plumes while also including a selection of nonduskside plumes, we can consider that the choice of plume intervals for our study is reasonably general. For each of the 14 chosen plumes, we present in Table 2 an average value for the hiss amplitude $\overline{\Delta B}$ (pT) calculated by averaging the measured spectral intensity along each plume crossing.

3. Theory

[16] From Summers [2005] (equations (10) and (17)), we can write the local pitch-angle diffusion coefficient for electron cyclotron resonance with field-aligned R-mode electromagnetic waves in the form

$$D_{\alpha\alpha} = \frac{\pi}{2} \frac{|\Omega_e|^2}{B_0^2} \frac{1}{(E+1)^2} \sum_{j=1}^N \left(1 - \frac{\omega_j \cos \alpha}{v k_j}\right)^2 \times \frac{I(k)}{|v \cos \alpha - d\omega_j/dk_j|} \quad (1)$$

for broadband waves of intensity $I(k)$ or $\hat{I}(f)$ (nT^2/Hz), defined on the frequency range $\omega_1 < \omega < \omega_2$, where

$$\Delta B^2 = \int_{-\infty}^{\infty} I(k) dk = \int_{f_1}^{f_2} \hat{I}(f) df, \quad (2)$$

and ΔB is the wave amplitude; $f = \omega/2\pi$, $f_1 = \omega_1/2\pi$, and $f_2 = \omega_2/2\pi$; α is the particle pitch angle and v is the particle speed; E is the dimensionless particle kinetic energy given by $E = E_k/(m_e c^2) = \gamma - 1$ where $\gamma = (1 - v^2/c^2)^{-1/2}$ is the Lorentz factor (c is the speed of light), and m_e is the electron rest mass; $|\Omega_e| = eB_0/(m_e c)$ is the electron gyrofrequency, where e is the unit charge and B_0 is the magnitude of the uniform static magnetic field; the wave frequency ω_j and wave number k_j (where $j = 1, 2, \dots, N$) satisfy the gyroresonance condition

$$\omega_j - v k_j \cos \alpha = |\Omega_e|/\gamma, \quad (3)$$

Table 2. Average Hiss Amplitude $\overline{\Delta B}$ (pT) Calculated by Averaging the Measured Spectral Intensity Along Each Chosen Plume Crossing

ORBIT	297	302	446 (Out)	446 (In)	605	672	673	674	810	869	871	939	941	977
$\overline{\Delta B}$ (pT)	14	16	48	27	42	25	13	37	91	34	60	203	31	102

as well as the dispersion relation,

$$\left(\frac{ck}{\omega}\right)^2 = 1 - \frac{(1 + \varepsilon)/\alpha^*}{(\omega/|\Omega_e| - 1)(\omega/|\Omega_e| + \varepsilon)}, \quad (4)$$

where

$$\alpha^* = \Omega_e^2/\omega_{pe}^2 \quad (5)$$

is an important cold-plasma parameter; $\varepsilon = m_e/m_p$ where m_p is the proton rest mass; and $\omega_{pe} = (4\pi N_0 e^2/m_e)^{1/2}$ is the plasma frequency where N_0 is the electron number density.

[17] It is convenient to express formula (1) in terms of the practical wave intensity $\hat{I}(f)$ (nT²/Hz). Then, also introducing the variables,

$$x = \omega_j/|\Omega_e|, \quad y = ck_j/|\Omega_e|, \quad (6)$$

we thereby obtain the result,

$$D_{\alpha\alpha} = \frac{1}{4} \frac{|\Omega_e|^2}{B_0^2} \frac{1}{(E+1)^2} \sum_{j=1}^N \left(1 - \frac{x \cos \alpha}{y\beta}\right)^2 \frac{\hat{I}(f) |F(x,y)|}{|\beta \cos \alpha - F(x,y)|}, \quad (7)$$

where (from (3))

$$y = (x - 1/\gamma)/(\beta \cos \alpha). \quad (8)$$

In (7), the function $F(x, y)$ is given by expression (C1) from *Summers* [2005]; $\beta = v/c = [E(E+2)]^{1/2}/(E+1)$; and x satisfies the quartic equation (A1) given also by *Summers* [2005].

[18] In order to apply (7) to the assumed dipole magnetic field of the inner magnetosphere, it remains to carry out bounce-averaging of (7) to take account of the magnetic mirror-like geometry. Using the formalism given by *Summers et al.* [2007a], we write the bounce-averaged diffusion coefficient $\langle D_{\alpha\alpha} \rangle$ as

$$\langle D_{\alpha\alpha} \rangle = \frac{1}{S(\alpha_{eq})} \int_0^{\lambda_m} D_{\alpha\alpha}(\alpha) \frac{\cos \alpha \cos^7 \lambda}{\cos^2 \alpha_{eq}} d\lambda, \quad (9)$$

where

$$S(\alpha_{eq}) = 1.3 - 0.56 \sin \alpha_{eq}. \quad (10)$$

In (9), α_{eq} is the equatorial pitch angle of a particle, and λ is the magnetic latitude of a particle with pitch-angle α at any point along a field line; α_{eq} , λ , and α satisfy the relation,

$$\sin^2 \alpha = f(\lambda) \sin^2 \alpha_{eq}, \quad (11)$$

where

$$f(\lambda) = (1 + 3 \sin^2 \lambda)^{1/2} / \cos^6 \lambda, \quad (12)$$

where λ_m is the latitude of the mirror point of the particle and is given by the equation,

$$X^6 + (3 \sin^4 \alpha_{eq})X - 4 \sin^4 \alpha_{eq} = 0, \quad (13)$$

with $X = \cos^2 \lambda_m$.

[19] We substitute the local diffusion coefficient $D_{\alpha\alpha}(\alpha)$ given by (7) into (9), and regard α as a function of α_{eq} and λ , as given by (11). Thus, the bounce-averaged diffusion coefficient $\langle D_{\alpha\alpha} \rangle$ is a function of α_{eq} . The background magnetic field B_0 occurring in $D_{\alpha\alpha}(\alpha)$ in (9) is replaced by the value

$$B_0 = B_{eq} f(\lambda), \quad (14)$$

where

$$B_{eq} = B_{local} / f(\lambda_{local}). \quad (15)$$

B_{eq} is the equatorial magnetic field, and B_{local} is the locally observed magnetic field at the observed magnetic latitude λ_{local} , corresponding to the observed L -value. In the absence of other data to show latitudinal variations in density, we assume that the background electron number density N_0 is constant along a field line ($N_0 = N_{eq} = N_{local}$). We likewise assume that the hiss spectral intensity is constant along a field line. From a statistical survey of CRRES data, *Meredith et al.* [2004] found that hiss peaks near the equatorial ($|\text{MLAT}| < 15^\circ$) and midlatitude ($15^\circ < |\text{MLAT}| < 30^\circ$) regions. CRRES data are not available at high latitudes ($|\text{MLAT}| > 30^\circ$). Our assumption that hiss is also present at high latitudes is partially justified by other studies. For example, *Thorne et al.* [1973], using OGO5 search coil magnetometer data, found that hiss was present on almost every pass through the plasmasphere. *Thorne et al.* [1973] found little distinction between lower latitude ($|\text{MLAT}| < 30^\circ$) and high-latitude ($|\text{MLAT}| > 30^\circ$) plasmaspheric hiss emissions, and concluded that properties of hiss remain largely constant throughout the plasmasphere. We make the assumption that hiss has constant spectral intensity along a field line on the basis of the best information available. Nevertheless, we recognize that if the wave power is confined to a lower range of latitudes then our calculations may overestimate the higher-energy loss rates since the waves resonate with higher-energy electrons at higher latitudes. Dependence of electron loss timescales on the latitudinal distribution of hiss, for a given energy and L -value, is examined by *Summers et al.* [2007b, section 3] and *Summers and Ni* [2008, section 3.2].

[20] Evaluation of the integral in (9) can be carried out by standard numerical quadrature which requires evaluation of the integrand at a set of λ -values (quadrature points) in the range $0 < \lambda < \lambda_m$. This requires, in particular, determination of the local diffusion coefficient $D_{\alpha\alpha}(\alpha)$ at the quadrature points. Therefore, at each quadrature point the relevant resonant roots x of the above-noted quartic equation must be found.

[21] We take as an estimate of the electron loss timescale,

$$\tau_{loss} = (1/\delta)(1/\langle D_{\alpha\alpha}^{LC} \rangle), \quad (16)$$

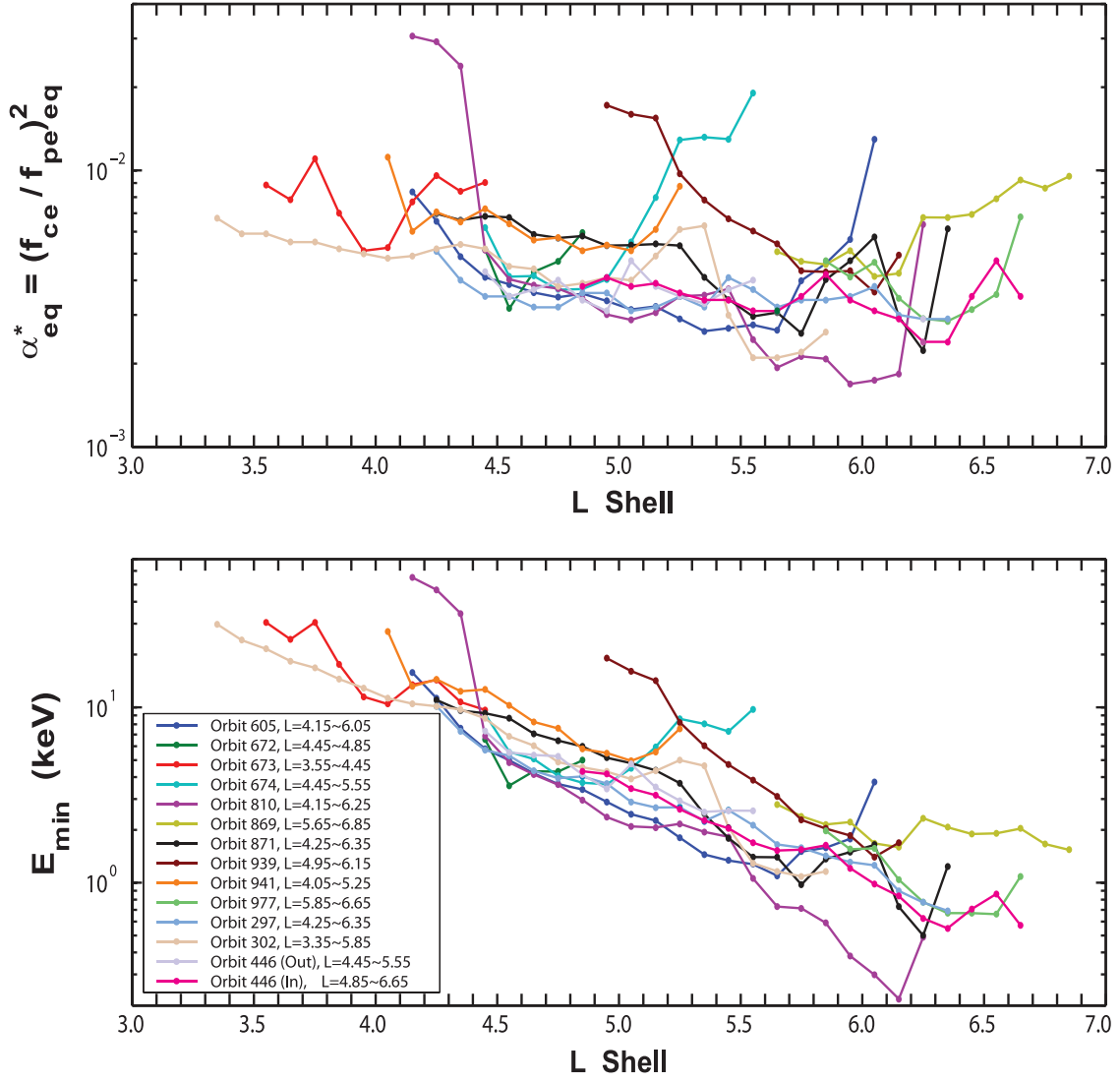


Figure 7. (top) Variation of the equatorial value of the parameter $\alpha^* = (f_{ce}/f_{pe})^2$ with L -value, for the specified plume intervals, inferred from local observed values of f_{ce} and f_{pe} . (bottom) Minimum energies for electron resonance with hiss at the frequency 1040 Hz, as a function of L -value, calculated using the values of α^* given in the top plot.

where $\langle D_{\alpha\alpha}^{LC} \rangle$ is the bounce-averaged diffusion coefficient (9) evaluated at $\alpha_{eq} = (\alpha_{LC})_{eq}$ where $(\alpha_{LC})_{eq}$ is the equatorial loss cone angle given by

$$\sin(\alpha_{LC})_{eq} = [L^5(4L - 3)]^{-1/4}. \quad (17)$$

In order to account for the limited angular (MLT) spread of the observed hiss in a given plume, we have inserted into (16) a drift-averaging factor δ which we specify in the following section. The value of τ_{loss} depends on the kinetic energy E , L -shell, the measured hiss spectral intensity \hat{I} , the drift-averaging factor δ , and the equatorial value of the parameter α^* , namely $\alpha_{eq}^* = (\Omega_e^2/\omega_{pe}^2)_{eq}$. The local electron gyrofrequency $|\Omega_e|$ was determined from the CRRES fluxgate magnetometer instrument [Singer *et al.*, 1992]. The local electron plasma frequency ω_{pe} was estimated from CRRES data on electrostatic waves at the upper hybrid frequency and the low-frequency cut-off of electromagnetic

continuum radiation, as described by Meredith *et al.* [2002]. In Figure 7 (top) we show the variation of α_{eq}^* with L -value, for the chosen plume intervals, deduced from local CRRES values for $|\Omega_e|$ and ω_{pe} . In Figure 7 (bottom) we show minimum electron energies for cyclotron resonance with hiss at the frequency 1040 Hz, as a function of L -value, corresponding to Figure 7 (top). The minimum resonant energy for electron resonance with hiss is obtained by setting $\sigma = e$ (for electrons) and $s = 1$ (for R-mode waves) in formula (16) of Summers *et al.* [2007a].

[22] As described in this section, the determination of the electron loss timescale τ_{loss} in our study assumes that the observed whistler-mode hiss is strictly field-aligned. CRRES data do not provide information on the wave-normal angle or angular spread of the waves. While the assumption that the waves are field-aligned is likely to be an approximation, we consider that our method for calculating τ_{loss} yields reasonably reliable results based on the relatively

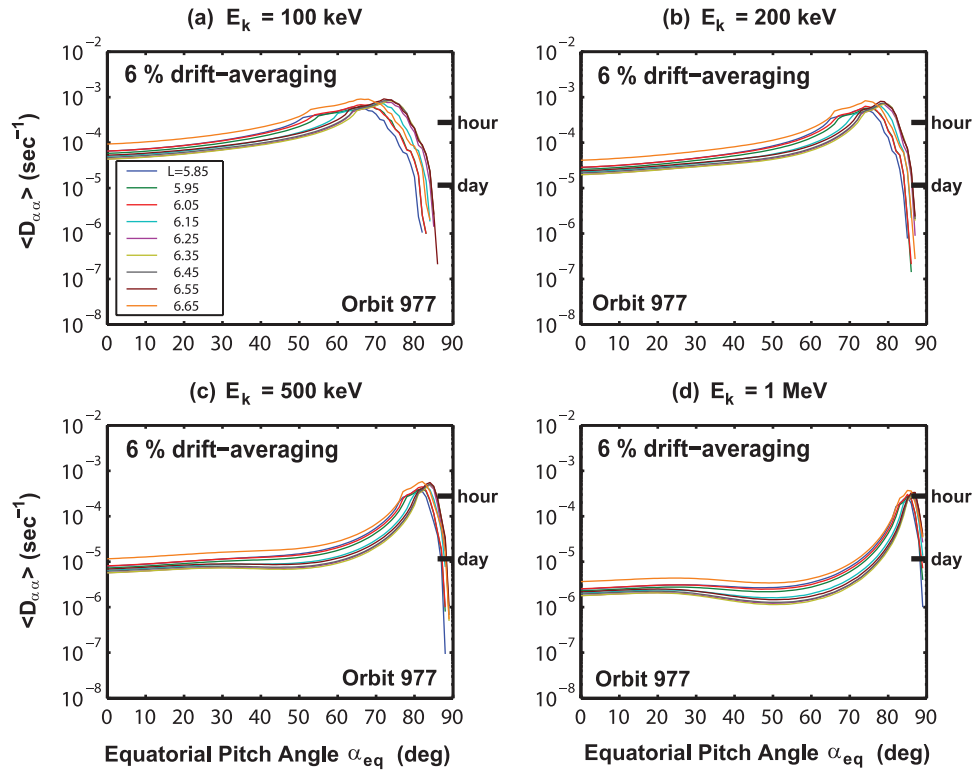


Figure 8. Bounce-averaged pitch-angle diffusion rates for electrons interacting with hiss during the chosen plume crossing for orbit 977, at the indicated L -values and electron energies. Hiss in the plume is assumed to be distributed along the whole field line.

limited available data. In support of our method, we cite the recent analysis by *Summers et al.* [2007b] who calculated electron loss timescales due to scattering by plasmaspheric hiss during low geomagnetic activity in the region $3 < L < 5$. *Summers et al.* [2007b] assumed field-aligned hiss with zero wave-normal distribution and predicted electron loss timescales in good agreement with the measured values obtained from CRRES Medium Electrons A data by *Meredith et al.* [2006a]. It should nevertheless be pointed out that inclusion of higher-order scattering could significantly alter the scattering rates near the edge of the loss cone if the hiss becomes strongly oblique. Specifically, we would expect increased loss timescales if the wave-normal angle is large, as demonstrated by *Meredith et al.* [2006a].

4. Electron Loss Timescales

[23] Electron loss timescales calculated in this paper must of course be considered in the context of plume lifetimes overall. Plumets have been observed over the duration of many consecutive CRRES orbits [e.g., see *Moldwin et al.*, 2004, Figure 8]. Since the CRRES orbital period is about 10 hours, this indicates that plumets can last from 10 hours to more than 1 day. Global imaging by the EUV imager of the IMAGE satellite has tracked the evolution of various plumets over several hours to more than 1 day [e.g., *Spasojević et al.*, 2003; *Goldstein et al.*, 2004]. Very few studies have measured the full global evolution of a plasmaspheric plume from its creation to its complete dissipation. It is possible that some plumets persist for several days. For practical purposes, we take an upper limit for the lifetime of

a plume to be 5 days, in which case a value of τ_{loss} exceeding 5 days indicates that electron scattering by hiss is ineffective for that particular plume at the L -shell and electron energy under consideration. Plume formations exceeding 5 days in duration are likely to consist of multiple plumets formed in succession. However, at geosynchronous orbit ($L \sim 6.6$) cold dense regions in narrow MLT channels are commonly observed over 10-day intervals or longer. In an investigation using multiple geosynchronous satellites, *Moldwin et al.* [1994] found that plasmaspheric plasma was absent on only 13% of the days in the study interval.

[24] For electrons of a given energy E , we determine the loss timescale τ_{loss} due to scattering by hiss at a given L -shell in a chosen plume as the inverse of the bounce-averaged diffusion coefficient $\langle D_{\alpha\alpha} \rangle$ evaluated at the equatorial loss cone angle (formulae (16)–(17)). An orbiting energetic electron traverses a plume only for a fraction of its orbit. To take account of the azimuthal (MLT) spread of a plume we have included a drift-averaging factor δ in (16). The azimuthal spread of a particular plume varies during its evolution and is typically $0.1 R_E$ to $1.5 R_E$ or more [e.g., *Spasojević et al.*, 2003; *Darrowzet et al.*, 2006]. Hereinafter, we take the drift-averaging factor δ as 6% since this appears to correspond approximately to the typical observed azimuthal width of a plume.

[25] *Shprits et al.* [2006a] recently analyzed the controlling effect of the pitch-angle scattering rates near the loss cone on energetic electron lifetimes, and found that the electron phase space density reaches an equilibrium shape within hours of the simulation when scattering rates do not

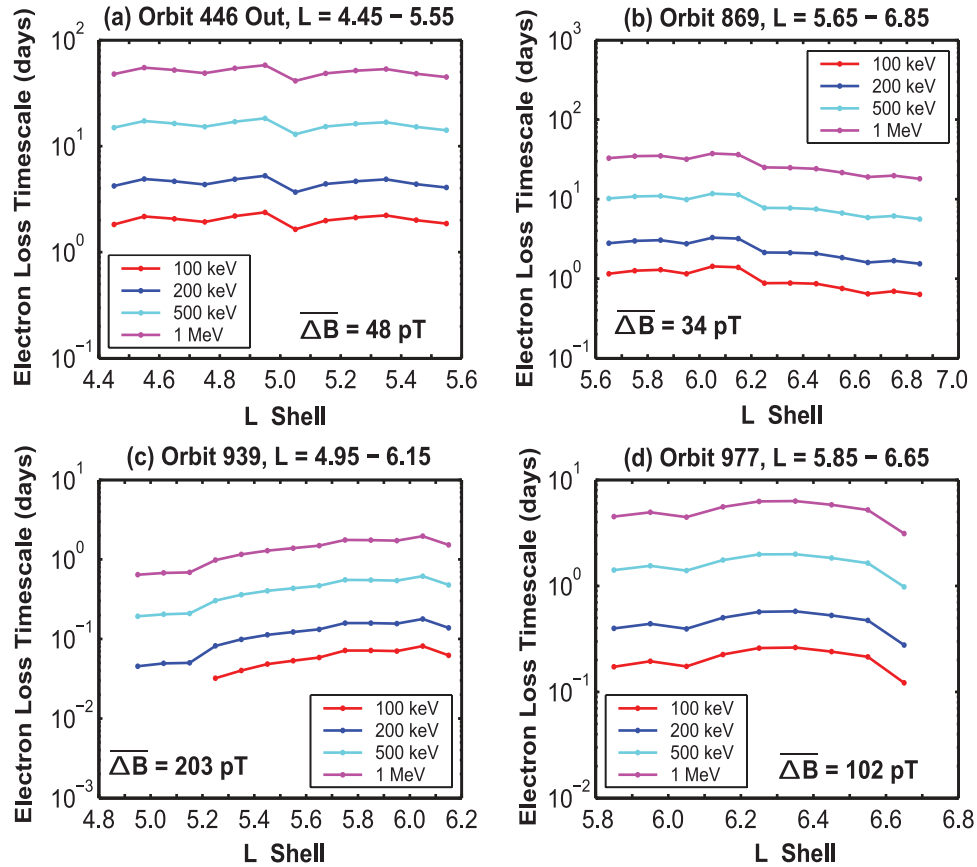


Figure 9. Electron loss timescales due to scattering by hiss at the specified energies, for the indicated CRRES plume crossings, as a function of L -value; 6% drift-averaging has been applied.

drop below 1/10 of the value near the edge of the loss cone for up to a 30° -wide range of pitch angles. In this case, electron lifetimes were found to be primarily controlled by scattering rates near the edge of the loss cone. Further, *Shprits et al.* [2006a] found that while a drop in the diffusion coefficients by a factor of 100 to 1000 near $\alpha_{eq} = 90^\circ$ results in weak scattering at high pitch angles, the lower pitch-angle particle distribution decays on a timescale comparable to that determined by the diffusion rate near the edge of the loss cone. Herein, we utilize the findings of *Shprits et al.* [2006a] and estimate electron loss timescales by using the scattering rate at the edge of the loss cone only in those cases in which the diffusion rate is small over a high pitch-angle range narrower than $75^\circ < \alpha_{eq} < 90^\circ$. By using this criterion, we expect that our reported timescales afford reasonable estimates of the decay times of at least the bulk of the electron distribution.

[26] In order to carry out accurate drift-averaging of the diffusion rates we require specification of the complete MLT distribution of hiss spectral intensity. However, only point measurements of the hiss intensity are made by CRRES at particular MLT values and specific L -shells as the satellite traverses each particular plume. We assume that the average wave power determined along the satellite track is a measure of the MLT wave distribution at a given L -value. Specifically, for each plume we average over all the measured profiles of the hiss spectral intensity, and we use this average intensity, together with the drift-averaging factor δ , to deter-

mine the MLT-averaged scattering rate at each L -shell. In Figure 8 we show examples of profiles of the bounce-averaged and drift-averaged electron diffusion coefficient $\langle D_{\alpha\alpha} \rangle$ for the plume interval in orbit 977 for electrons of energies 100 keV, 200 keV, 500 keV, and 1 MeV, at the given L -shells. We plot the electron loss timescale τ_{loss} at the specified energies as a function of L -shell for the chosen plumes in orbits 446 (Out), 869, 939, and 977 in Figures 9a, 9b, 9c, and 9d, respectively. Hiss intensity for orbit 446 (Out) is the strongest of the 4 nonduskside plume crossings, and hiss intensities during orbits 869, 939, and 977 are among the strongest in the 10 duskside plume crossings (see Figure 6 and Table 2). From Figure 9, and the corresponding figures for the other 10 plumes not shown, we deduce that at a fixed L -shell, τ_{loss} increases as the electron kinetic energy increases from 100 keV to 1 MeV. It is also evident from Figure 9 that scattering by hiss in plumes can be especially effective for electrons of energy 100–200 keV. For instance, for the plume in orbit 977 (Figure 9d), for which the average wave amplitude $\overline{\Delta B} = 102$ pT, τ_{loss} ranges from 2.9 to 6.3 hr for 100 keV electrons, and from 6.6 to 13.8 hr for 200 keV electrons. For the plume in orbit 939 (Figure 9c), for which the wave intensity is strong ($\overline{\Delta B} = 203$ pT), the minimum loss timescale $(\tau_{loss})_{min}$ is 0.7 hr for 100 keV electrons and 1.1 hr for 200 keV electrons. For orbit 869 (Figure 9b), $\overline{\Delta B} = 34$ pT, minimum timescales are $(\tau_{loss})_{min} = 15.2, 36.9$ hr for 100 keV, 200 keV electrons, and for orbit 446

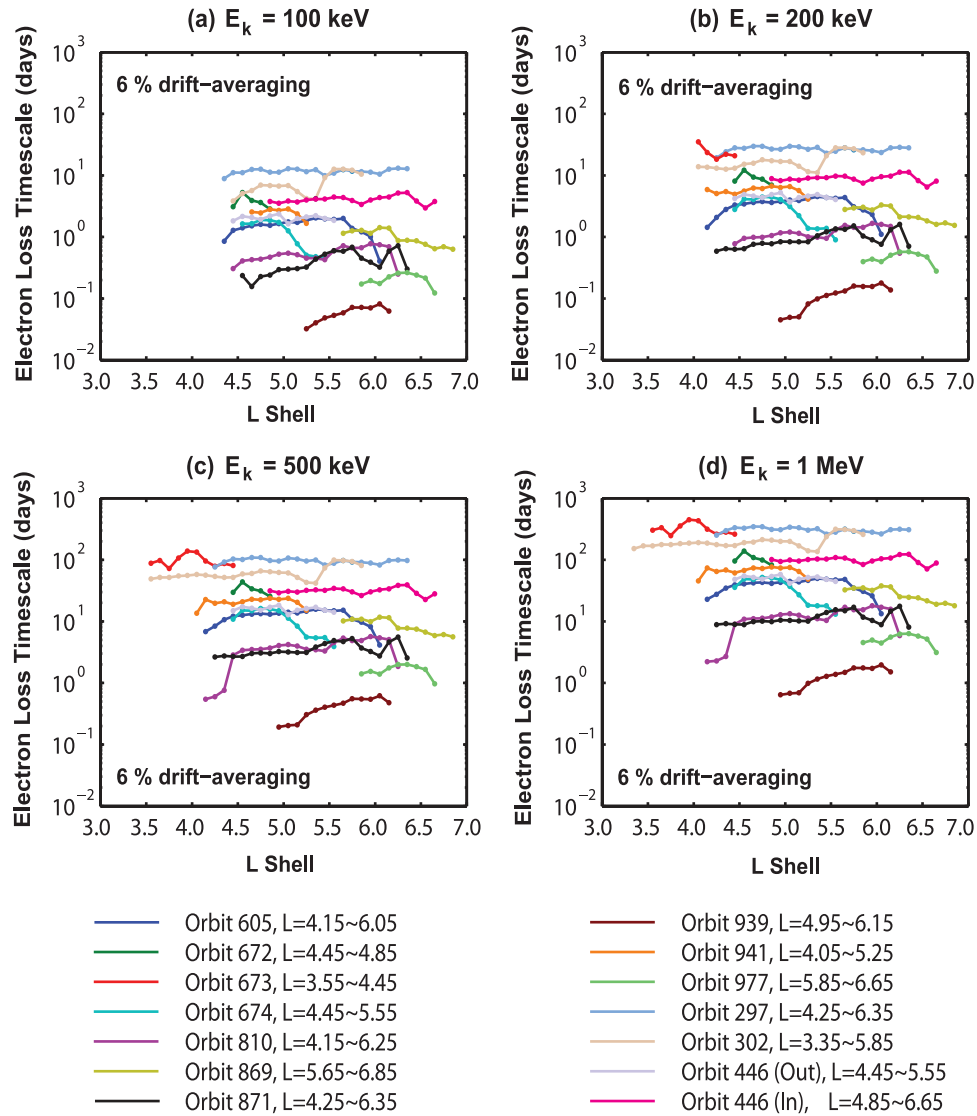


Figure 10. Summary plot of electron loss timescales due to scattering by hiss at the specified energies, for each of the 14 chosen CRRES plume crossings, as a function of L -value.

(Out) (Figure 9a, $\overline{\Delta B} = 48$ pT) we find $(\tau_{loss})_{min} = 1.6, 3.7$ days for 100 keV, 200 keV electrons.

[27] We can also see from Figure 9 that, in general, scattering by hiss in plumes is somewhat less effective for 500 keV electrons, and still more ineffective for 1 MeV electrons. Minimum loss timescales for the plumes in orbits 977, 869, and 446 are respectively $(\tau_{loss})_{min} = 1, 5.6,$ and 13 days, for 500 keV electrons. Corresponding respective values for 1 MeV electrons are $(\tau_{loss})_{min} = 3.1, 18,$ and 41 days. Particularly rapid scattering of 500 keV to 1 MeV electrons by hiss in plumes is possible, but only in the case of intense waves. For example, for the plume in orbit 939, $(\tau_{loss})_{min} = 4.6$ hr for 500 keV electrons and $(\tau_{loss})_{min} = 15.4$ hr for 1 MeV electrons.

[28] We plot the loss timescales for electrons of energy 100 keV, 200 keV, 500 keV, and 1 MeV, as a function of L -shell, in the Figures 10a, 10b, 10c, and 10d, respectively, for all the 14 chosen plumes in our study. Complementary to Figure 10, we list in Table 3 the number of the chosen plumes

for which electrons at each of the energies 100 keV, 200 keV, 500 keV, and 1 MeV, have a loss timescale less than the specified values (0.1, 0.5, 1, and 2 days) at some L -shells. Figure 10 and Table 3 essentially summarize the results of our calculations of τ_{loss} for our total selection of plumes. The decrease in efficiency of scattering by hiss as electron energies increase from 100 keV to 1 MeV is confirmed in Figure 10 by the general upward shift of the timescale profiles from Figure 10a through to Figure 10d. Likewise, the number of profiles (or portions of profiles) located above $\tau_{loss} = 5$ days, the nominal timescale above which scattering is ineffective in plumes, progressively increases from Figure 10a through to Figure 10d. The degree of effectiveness of electron scattering by hiss at each of the energies 100 keV, 200 keV, 500 keV, and 1 MeV can be particularly appreciated by viewing each of Figures 10a–10d with each corresponding column of Table 3. For instance, for 100 keV electrons scattering is fairly rapid ($\tau_{loss} < 0.5$ day) at some L -shells in 6 of the 14 chosen

Table 3. Number of the 14 Chosen Plumets for Which Electrons at the Indicated Energy Have a Loss Timescale Less Than the Specified Value at Some L -Shells

	100 keV	200 keV	500 keV	1 MeV
$\tau_{loss} < 2$ day (some L)	9	7	3	1
$\tau_{loss} < 1$ day (some L)	7	5	2	1
$\tau_{loss} < 0.5$ day (some L)	6	2	1	0
$\tau_{loss} < 0.1$ day (some L)	1	1	0	0

plumes. Further, in 9 plumes scattering of 100 keV electrons can be regarded as at least moderately effective ($\tau_{loss} < 2$ days) at some L -shells. It is also useful to examine the entries in each particular row of Table 3 separately. For example, the number of plumes for which $\tau_{loss} < 1$ day, at some L -shells, progressively decreases from 7 to 1 as the electron energy increases from 100 keV to 1 MeV. The scattering of MeV electrons in less than 1 day appears to require hiss amplitudes well in excess of 100 pT. Such a statement is not straightforward to qualify accurately, however, since τ_{loss} depends in a complicated way on the various parameters occurring in the formula for the diffusion coefficient (7).

[29] Of the 14 chosen plumes, 6 contain at least reasonably intense hiss, specifically with an average wave amplitude satisfying $\Delta B \geq 42$ pT (see Table 2). The plume in orbit 939, with $\Delta B = 203$ pT, contains the most intense hiss. We have also selected 3 plumes with relatively weak hiss, satisfying $\Delta B \leq 16$ pT. Electron scattering in these plumes (in orbits 297, 302, and 673) is naturally likewise weak, in general, with minimum values of τ_{loss} of at least several days.

[30] Overall, it is clear from the numerical results reported in this section that, under appropriate conditions, hiss in plumes can induce significant precipitation losses of energetic (100 keV to 1 MeV) electrons in the outer zone, $3 < L < 7$.

5. Discussion

[31] This is the first study to quantify the contribution of pitch-angle scattering by whistler-mode hiss in plumes to the total precipitation loss of outer-zone energetic electrons using experimental wave data in observed plumes. Understanding the acceleration and loss mechanisms of radiation belt electrons is needed to develop models for nowcasting and forecasting of relativistic (>1 MeV) electrons that are a potential danger to satellites and humans in space. A primary objective of the twin-spacecraft NASA Radiation Belt Storm Probes (RBSP) mission [Kintner and the Living With a Star Geospace Mission Definition Team, 2002] and the proposed Canadian Outer Radiation Belt Injection, Transport, Acceleration and Loss Satellite (ORBITALS) mission [Mann et al., 2006] is to understand the physical processes that control the dynamical variation of outer radiation belt electron fluxes. Wave-particle interactions undoubtedly play a crucial role in radiation belt electron dynamics. Electron gyroresonance with VLF chorus can lead to stochastic acceleration of seed (~ 100 keV) electrons to MeV energies in the low-density regions outside the plasmasphere and plasmaspheric plumes [Summers et al., 1998, 2002, 2004, 2007b; Horne and Thorne, 1998; Roth et al., 1999; Summers and Ma, 2000; Meredith et al., 2002, 2003a; Miyoshi et al., 2003; Horne et al., 2005a, 2005b;

Varotsou et al., 2005; Omura and Summers, 2006; Shprits et al., 2006b; Li et al., 2007]. Relativistic (>1 MeV) electrons just outside the plasmapause can be scattered by VLF chorus into the loss cone, on timescales of a day, and observed at low altitudes as microburst precipitation [Lorentzen et al., 2001; Thorne et al., 2005]. Scattering by EMIC waves along the duskside plasmasphere can induce precipitation loss of MeV electrons on timescales of several hours to a day [Lorentzen et al., 2000; Summers and Thorne, 2003; Meredith et al., 2003b; Summers et al., 2007b]. In the present study we have shown that whistler-mode hiss in plumes can likewise induce precipitation loss of MeV electrons in a day or less, though only in the case of exceptionally strong waves (typically with amplitude 100's pT). Of particular interest in our study is the finding that electrons of energy 100–200 keV, which are required to form a seed population from which MeV electrons are generated, can suffer rapid precipitation loss (in a time-scale of hours) due to scattering by hiss in plumes. Thus, while scattering by hiss in plumes may not usually induce rapid precipitation loss of MeV electrons, hiss scattering may reduce the generation of MeV electrons by depleting the seed electron population. The general conclusion to our study is that pitch-angle scattering by hiss in plumes in the frequency range $104 < f < 1040$ Hz can be efficient for inducing precipitation loss of outer-zone electrons with energies throughout the range 100 keV to 1 MeV. However, the results in section 4 show that the magnitude of the precipitation loss timescale can be highly dependent on wave power, L -value, and electron energy. Further, pitch-angle scattering rates can be sensitive to wave-normal angle and the latitudinal distributions of density and wave power. The precipitation loss timescales computed in this paper could be conservatively regarded as lower bounds.

[32] The competition between acceleration and loss of energetic electrons is determined by wave-particle interactions taking place outside and inside the dense thermal regions comprising the plasmasphere and plasmaspheric plumes. Acceleration and loss of energetic electrons due to gyroresonance with whistler-mode chorus take place outside these thermal regions, while precipitation loss due to pitch-angle scattering by hiss and EMIC waves takes place inside the thermal regions. The generation and global distribution of energetic electrons in the outer zone is therefore greatly influenced by the distribution of thermal plasma. Accurate modeling of the dynamical variation of the outer radiation belt electron flux requires knowledge of the spectral intensity and temporal variation of the appropriate wave modes both inside and outside the thermal plasma regions.

[33] **Acknowledgments.** This work is supported by the Natural Sciences and Engineering Research Council of Canada under grant A-0621. Additional support is acknowledged from NSF grant ATM 0402615. Part of this project was carried out when D. S. was Visiting Scholar in the Department of Physics and Technology, University of Bergen, Norway; D. S. thanks the University of Bergen, and especially Finn Soraas, for the excellent hospitality.

[34] Zuyin Pu thanks the reviewers for their assistance in evaluating the manuscript.

References

Abel, B., and R. M. Thorne (1998), Electron scattering loss in Earth's inner magnetosphere: 1. Dominant physical processes, *J. Geophys. Res.*, *103*, 2385.

- Albert, J. M. (1994), Quasi-linear pitch angle diffusion coefficients: Retaining high harmonics, *J. Geophys. Res.*, *99*, 23,741.
- Albert, J. M. (2003), Evaluation of quasi-linear diffusion coefficients for EMIC waves in a multispecies plasma, *J. Geophys. Res.*, *108*(A6), 1249, doi:10.1029/2002JA009792.
- Anderson, R. R., D. A. Gurnett, and D. L. Odem (1992), CRRES plasma wave experiment, *J. Spacecr. Rockets*, *29*, 570.
- Baker, D. N., S. G. Kanekal, X. Li, S. P. Monk, J. Goldstein, and J. L. Burch (2004), An extreme distortion of the Van Allen belt arising from the Halloween solar storm in 2003, *Nature*, *432*, 878.
- Burch, J. L. (2006), New insights on magnetospheric processes from IMAGE, paper presented at Conference on Earth-Sun System Exploration: Energy Transfer, Johns Hopkins Univ. Appl. Phys. Lab., Kona, Hawaii.
- Burch, J. L., W. S. Lewis, T. J. Immel, P. C. Anderson, H. U. Frey, S. A. Fuselier, J. C. Gerard, S. B. Mende, D. G. Mitchell, and M. F. Thomsen (2002), Interplanetary magnetic field control of aftermoon-sector detached proton auroral arcs, *J. Geophys. Res.*, *107*(A9), 1251, doi:10.1029/2001JA007554.
- Carpenter, D. L. (1963), Whistler evidence of a "knee" in the magnetospheric ionization density profile, *J. Geophys. Res.*, *68*, 1675.
- Carpenter, D. L., and R. R. Anderson (1992), An ISEE/whistler model of equatorial electron density in the magnetosphere, *J. Geophys. Res.*, *97*, 1097.
- Carpenter, D. L., and J. Lemaire (1997), Erosion and recovery of the plasmasphere in the plasmopause region, *Space Sci. Rev.*, *80*, 153.
- Carpenter, D. L., and C. G. Park (1973), On what ionospheric workers should know about the plasmopause-plasmasphere, *Rev. Geophys.*, *11*(1), 133.
- Chan, K. W., and R. E. Holzer (1976), ELF hiss associated with plasma density enhancements in the outer magnetosphere, *J. Geophys. Res.*, *81*, 2267.
- Chappell, C. R. (1974), Detached plasma regions in the magnetosphere, *J. Geophys. Res.*, *79*, 1861.
- Chappell, C. R., K. K. Harris, and G. W. Sharp (1970), The morphology of the bulge region of the plasmasphere, *J. Geophys. Res.*, *75*, 3848.
- Cornilleau-Wehrin, N., R. Gendrin, F. Lefeuvre, M. Parrot, R. Gard, D. Jones, A. Bahnsen, E. Ungstrup, and W. Gibbons (1978), VLF electromagnetic waves observed onboard GEOS-1, *Space Sci. Rev.*, *22*, 371.
- Darrouzet, F., et al. (2006), Analysis of plasmaspheric plumes: CLUSTER and IMAGE observations, *Ann. Geophys.*, *24*, 1737.
- Dent, Z. C., I. R. Mann, J. Goldstein, F. W. Menk, and L. G. Ozeke (2006), Plasmaspheric depletion, refilling, and plasmopause dynamics: A coordinated ground-based and IMAGE satellite study, *J. Geophys. Res.*, *111*, A03205, doi:10.1029/2005JA011046.
- Draganov, A. B., U. S. Inan, V. S. Sonwalkar, and T. F. Bell (1992), Magnetically reflected whistlers as a source of plasmaspheric hiss, *Geophys. Res. Lett.*, *19*, 233.
- Etcheto, J., R. Gendrin, J. Solomon, and A. Roux (1973), A self-consistent theory of magnetospheric ELF hiss, *J. Geophys. Res.*, *78*, 8150.
- Ganguli, G., M. A. Reynolds, and M. W. Liemohn (2000), The plasmasphere and advances in plasmaspheric research, *J. Atmos. Solar Terr. Phys.*, *62*, 1647.
- Goldstein, J. (2006), Plasmasphere response: tutorial and review of recent imaging results, *Space Sci. Rev.*, *124*, 203, doi:10.1007/s11214-006-9105-y.
- Goldstein, J., B. R. Sandel, P. H. Reiff, and M. R. Hairston (2003), Control of plasmaspheric dynamics by both convection and sub-auroral polarization stream, *Geophys. Res. Lett.*, *30*(24), 2243, doi:10.1029/2003GL018390.
- Goldstein, J., B. R. Sandel, M. F. Thomsen, M. Spasojević, and P. H. Reiff (2004), Simultaneous remote sensing and in situ observations of plasmaspheric drainage plumes, *J. Geophys. Res.*, *109*, A03202, doi:10.1029/2003JA010281.
- Goldstein, J., B. R. Sandel, W. T. Forrester, M. F. Thomsen, and M. R. Hairston (2005), Global plasmasphere evolution 22–23 April 2001, *J. Geophys. Res.*, *110*, A12218, doi:10.1029/2005JA011282.
- Green, J. L., S. Boardsen, L. Garcia, W. W. L. Taylor, S. F. Fung, and B. W. Reinisch (2005), On the origin of whistler mode radiation in the plasmasphere, *J. Geophys. Res.*, *110*, A03201, doi:10.1029/2004JA010495.
- Green, J. L., S. Boardsen, L. Garcia, S. F. Fung, and B. W. Reinisch (2006), Reply to Comment on "On the origin of whistler mode radiation in the plasmasphere" by Green et al., *J. Geophys. Res.*, *111*, A09211, doi:10.1029/2006JA011622.
- Hayakawa, M., and S. S. Sazhin (1992), Mid-latitude and plasmaspheric hiss: A review, *Planet. Space Sci.*, *40*, 1325.
- Hayakawa, M., N. Ohmi, M. Parrot, and F. Lefeuvre (1986), Direction finding of ELF hiss emissions in a detached plasma region of the magnetosphere, *J. Geophys. Res.*, *91*, 135.
- Horne, R. B., and R. M. Thorne (1998), Potential waves for relativistic electron scattering and stochastic acceleration during magnetic storms, *Geophys. Res. Lett.*, *25*, 3011.
- Horne, R. B., R. M. Thorne, S. A. Glauert, J. M. Albert, N. P. Meredith, and R. R. Anderson (2005a), Timescale for radiation belt electron acceleration by whistler mode chorus waves, *J. Geophys. Res.*, *110*, A03225, doi:10.1029/2004JA010811.
- Horne, R. B., et al. (2005b), Wave acceleration of electrons in the Van Allen radiation belts, *Nature*, *437*, 227, doi:10.1038/nature03939.
- Horwitz, J. L., R. H. Comfort, and C. R. Chappell (1990), A statistical characterization of plasmasphere structure and boundary locations, *J. Geophys. Res.*, *95*, 7937.
- Huang, C. Y., C. K. Goertz, and R. R. Anderson (1983), A theoretical study of plasmaspheric hiss generation, *J. Geophys. Res.*, *88*, 7927.
- Kintner, P. M., and the Living With a Star Geospace Mission Definition Team, (2002), The LWS geospace tech investigations: Exploring the extremes of space weather, *NASA Tech. Memo.*, *TM-2002-211613*.
- Lemaire, J. F., and K. I. Gringauz (1998), *The Earth's Plasmasphere*, Cambridge Univ. Press, New York.
- Li, W., Y. Y. Shprits, and R. M. Thorne (2007), Dynamic evolution of energetic outer zone electrons due to wave-particle interactions during storms, *J. Geophys. Res.*, *112*, A10220, doi:10.1029/2007JA012368.
- Lorentzen, K. R., M. P. McCarthy, G. K. Parks, J. E. Foat, R. M. Millan, D. M. Smith, R. P. Lin, and J. P. Treilhou (2000), Precipitation of relativistic electrons by interaction with electromagnetic ion cyclotron waves, *J. Geophys. Res.*, *105*, 5381.
- Lorentzen, K. R., J. B. Blake, U. S. Inan, and J. Bortnik (2001), Observations of relativistic electron microbursts in association with VLF chorus, *J. Geophys. Res.*, *106*, 6017.
- Lyons, L. R., and R. M. Thorne (1973), Equilibrium structure of radiation belt electrons, *J. Geophys. Res.*, *78*, 2142.
- Lyons, L. R., R. M. Thorne, and C. F. Kennel (1972), Pitch-angle diffusion of radiation belt electrons within the plasmasphere, *J. Geophys. Res.*, *77*, 3455.
- Mann, I. R., et al. (2006), The Outer Radiation Belt Injection, Transport, Acceleration and Loss Satellite (ORBITALS): A Canadian small satellite mission for ILWS, *Adv. Space Res.*, *38*, 1838.
- Masson, A., U. S. Inan, H. Laakso, O. Santolik, and P. Decreau (2004), Cluster observations of mid-latitude hiss near the plasmopause, *Ann. Geophys.*, *22*, 2565.
- Meredith, N. P., R. B. Horne, D. Summers, R. M. Thorne, R. H. A. Iles, D. Heynderickx, and R. R. Anderson (2002), Evidence for acceleration of outer zone electrons to relativistic energies by whistler mode chorus, *Ann. Geophys.*, *20*, 967.
- Meredith, N. P., M. Cain, R. B. Horne, R. M. Thorne, D. Summers, and R. R. Anderson (2003a), Evidence for chorus-driven electron acceleration to relativistic energies from a survey of geomagnetically disturbed periods, *J. Geophys. Res.*, *108*(A6), 1248, doi:10.1029/2002JA009764.
- Meredith, N. P., R. M. Thorne, R. B. Horne, D. Summers, B. J. Fraser, and R. R. Anderson (2003b), Statistical analysis of relativistic electron energies for cyclotron resonance with EMIC waves observed on CRRES, *J. Geophys. Res.*, *108*(A6), 1250, doi:10.1029/2002JA009700.
- Meredith, N. P., R. B. Horne, R. M. Thorne, D. Summers, and R. R. Anderson (2004), Substorm dependence of plasmaspheric hiss, *J. Geophys. Res.*, *109*, A06209, doi:10.1029/2004JA010387.
- Meredith, N. P., R. B. Horne, S. A. Glauert, R. M. Thorne, D. Summers, J. M. Albert, and R. R. Anderson (2006a), Energetic outer zone electron loss timescales during low geomagnetic activity, *J. Geophys. Res.*, *111*, A05212, doi:10.1029/2005JA011516.
- Meredith, N. P., R. B. Horne, M. A. Clilverd, D. Horsfall, R. M. Thorne, and R. R. Anderson (2006b), Origins of plasmaspheric hiss, *J. Geophys. Res.*, *111*, A09217, doi:10.1029/2006JA011707.
- Miyoshi, Y., A. Morioka, T. Obara, H. Misawa, T. Nagai, and Y. Kasahara (2003), Rebuilding process of the outer radiation belt during the 3 November 1993 magnetic storm: NOAA and Exos-D observations, *J. Geophys. Res.*, *108*(A1), 1004, doi:10.1029/2001JA007542.
- Moldwin, M. B., M. F. Thomsen, S. J. Bame, D. J. McComas, and K. R. Moore (1994), An examination of the structure and dynamics of the outer plasmasphere using multiple geosynchronous satellites, *J. Geophys. Res.*, *99*, 11,475.
- Moldwin, M. B., L. Downward, H. K. Rassoul, R. Amin, and R. R. Anderson (2002), A new model of the location of the plasmopause: CRRES results, *J. Geophys. Res.*, *107*(A11), 1339, doi:10.1029/2001JA009211.
- Moldwin, M. B., J. Howard, J. Sanny, J. D. Bocchicchio, H. K. Rassoul, and R. R. Anderson (2004), Plasmaspheric plumes: CRRES observations of enhanced density beyond the plasmopause, *J. Geophys. Res.*, *109*, A05202, doi:10.1029/2003JA010320.
- Omura, Y., and D. Summers (2006), Dynamics of high-energy electrons interacting with whistler mode chorus emissions in the magnetosphere, *J. Geophys. Res.*, *111*, A09222, doi:10.1029/2006JA011600.

- Parrot, M., and F. Lefeuvre (1986), Statistical study of the propagation characteristics of ELF hiss observed on GEOS-1, inside and outside the plasmasphere, *Ann. Geophys.*, *4*, 363.
- Roth, I., M. Temerin, and M. K. Hudson (1999), Resonant enhancement of relativistic electron fluxes during geomagnetically active periods, *Ann. Geophys.*, *17*, 631.
- Sandel, B. R., J. Goldstein, D. L. Gallagher, and M. Spasojević (2003), Extreme Ultraviolet Imager observations of the structure and dynamics of the plasmasphere, *Space Sci. Rev.*, *109*, 25.
- Santolik, O., M. Parrot, L. R. O. Storey, J. S. Pickett, and D. A. Gurnett (2001), Propagation analysis of plasmaspheric hiss using Polar PWI measurements, *Geophys. Res. Lett.*, *28*, 1127.
- Sheeley, B. W., M. B. Moldwin, H. K. Rassoul, and R. R. Anderson (2001), An empirical plasmasphere and trough density model: CRRES observations, *J. Geophys. Res.*, *106*, 25,631.
- Shprits, Y. Y., W. Li, and R. M. Thorne (2006a), Controlling effect of the pitch angle scattering rates near the edge of the loss cone on electron lifetimes, *J. Geophys. Res.*, *111*, A12206, doi:10.1029/2006JA011758.
- Shprits, Y. Y., R. M. Thorne, R. B. Horne, S. A. Glauert, M. Cartwright, C. T. Russell, D. N. Baker, and S. G. Kanekal (2006b), Acceleration mechanism responsible for the formation of the new radiation belt during the 2003 Halloween solar storm, *Geophys. Res. Lett.*, *33*, L05104, doi:10.1029/2005GL024256.
- Singer, H. J., W. P. Sullivan, P. Anderson, F. Mozer, P. Harvey, J. Wygant, and W. McNeil (1992), Fluxgate magnetometer instrument on the CRRES, *J. Spacecr. Rockets*, *29*, 599.
- Smith, E. J., A. M. A. Frandsen, B. T. Tsurutani, R. M. Thorne, and K. W. Chan (1974), Plasmaspheric hiss intensity variations during magnetic storms, *J. Geophys. Res.*, *79*, 2507.
- Sonwalkar, V. S., and U. S. Inan (1989), Lightning as an embryonic source of VLF hiss, *J. Geophys. Res.*, *94*, 6986.
- Spasojević, M., J. Goldstein, D. L. Carpenter, U. S. Inan, B. R. Sandel, M. B. Moldwin, and B. W. Reinisch (2003), Global response of the plasmasphere to a geomagnetic disturbance, *J. Geophys. Res.*, *108*(A9), 1340, doi:10.1029/2003JA009987.
- Spasojević, M., H. U. Frey, M. F. Thomsen, S. A. Fuselier, S. P. Gary, B. R. Sandel, and U. S. Inan (2004), The link between a detached subauroral proton arc and a plasmaspheric plume, *Geophys. Res. Lett.*, *31*, L04803, doi:10.1029/2003GL018389.
- Summers, D. (2005), Quasi-linear diffusion coefficients for field-aligned electromagnetic waves with applications to the magnetosphere, *J. Geophys. Res.*, *110*, A08213, doi:10.1029/2005JA011159.
- Summers, D., and C. Ma (2000), A model for generating relativistic electrons in the Earth's inner magnetosphere based on gyroresonant wave-particle interactions, *J. Geophys. Res.*, *105*, 2625.
- Summers, D., and B. Ni (2008), Effects of latitudinal distributions of particle density and wave power on cyclotron resonant diffusion rates of radiation belt electrons, *Earth Planets Space*, in press.
- Summers, D., and R. M. Thorne (2003), Relativistic electron pitch-angle scattering by electromagnetic ion cyclotron waves during geomagnetic storms, *J. Geophys. Res.*, *108*(A4), 1143, doi:10.1029/2002JA009489.
- Summers, D., R. M. Thorne, and F. Xiao (1998), Relativistic theory of wave-particle resonant diffusion with application to electron acceleration in the magnetosphere, *J. Geophys. Res.*, *103*, 20,487.
- Summers, D., C. Ma, N. P. Meredith, R. B. Horne, R. M. Thorne, D. Heynderickx, and R. R. Anderson (2002), Model of the energization of outer-zone electrons by whistler-mode chorus during the October 9, 1990 geomagnetic storm, *Geophys. Res. Lett.*, *29*(24), 2174, doi:10.1029/2002GL016039.
- Summers, D., C. Ma, N. P. Meredith, R. B. Horne, R. M. Thorne, and R. R. Anderson (2004), Modeling outer-zone relativistic electron response to whistler-mode chorus activity during substorms, *J. Atmos. Solar Terr. Phys.*, *66*, 133.
- Summers, D., B. Ni, and N. P. Meredith (2007a), Timescales for radiation belt electron acceleration and loss due to resonant wave-particle interactions: 1. Theory, *J. Geophys. Res.*, *112*, A04206, doi:10.1029/2006JA011801.
- Summers, D., B. Ni, and N. P. Meredith (2007b), Timescales for radiation belt electron acceleration and loss due to resonant wave-particle interactions: 2. Evaluation for VLF chorus, ELF hiss, and EMIC waves, *J. Geophys. Res.*, *112*, A04207, doi:10.1029/2006JA011993.
- Taylor, H. A., Jr., J. M. Grebowsky, and W. J. Walsh (1971), Structured variations of the plasmopause: Evidence of a corotating plasma tail, *J. Geophys. Res.*, *76*, 6806.
- Thorne, R. M., E. J. Smith, R. K. Burton, and R. E. Holzer (1973), Plasmaspheric hiss, *J. Geophys. Res.*, *78*, 1581.
- Thorne, R. M., E. J. Smith, K. J. Fiske, and S. R. Church (1974), Intensity variation of ELF hiss and chorus during isolated substorms, *Geophys. Res. Lett.*, *1*, 193.
- Thorne, R. M., S. R. Church, and D. J. Gorney (1979), On the origin of plasmaspheric hiss: The importance of wave propagation and the plasmopause, *J. Geophys. Res.*, *84*, 5241.
- Thorne, R. M., T. P. O'Brien, Y. Y. Shprits, D. Summers, and R. B. Horne (2005), Timescale for MeV electron microburst loss during geomagnetic storms, *J. Geophys. Res.*, *110*, A09202, doi:10.1029/2004JA010882.
- Thorne, R. M., R. B. Horne, and N. P. Meredith (2006), Comment on "On the origin of whistler mode radiation in the plasmasphere" by Green et al., *J. Geophys. Res.*, *111*, A09210, doi:10.1029/2005JA011477.
- Tsurutani, B. T., E. J. Smith, and R. M. Thorne (1975), Electromagnetic hiss and relativistic electron losses in the inner zone, *J. Geophys. Res.*, *80*, 600.
- Varotsou, A., D. Boscher, S. Bourdarie, R. B. Horne, S. A. Glauert, and N. P. Meredith (2005), Simulation of the outer radiation belt electrons near geosynchronous orbit including both radial diffusion and resonant interaction with whistler-mode chorus waves, *Geophys. Res. Lett.*, *32*, L19106, doi:10.1029/2005GL023282.

R. R. Anderson, Department of Physics and Astronomy, University of Iowa, Iowa City, IA 52242-1479, USA. (roger-r-anderson@uiowa.edu)

R. B. Horne and N. P. Meredith, British Antarctic Survey, Natural Environment Research Council, Madingley Road, Cambridge CB3 0ET, UK. (r.horne@bas.ac.uk; nmer@bas.ac.uk)

M. B. Moldwin, Institute of Geophysics and Planetary Physics and Department of Earth and Space Sciences, University of California, Los Angeles, 405 Hilgard Avenue, Los Angeles, CA 90095-1567, USA. (mmoldwin@igpp.ucla.edu)

B. Ni and D. Summers, Department of Mathematics and Statistics, Memorial University of Newfoundland, St. John's, NL, Canada A1C 5S7. (bbni@math.mun.ca; dsummers@math.mun.ca)

R. M. Thorne, Department of Atmospheric and Oceanic Sciences, University of California, Los Angeles, 405 Hilgard Avenue, Los Angeles, CA 90095-1567, USA. (rmt@atmos.ucla.edu)